Simultaneous Inhibition of the Arp2/3 Complex and Formins Enhances *de novo* Actin Filament Nucleation in *Arabidopsis thaliana*

Liyuan Xu[1], Lingyan Cao[1], Jiejie Li[1], Christopher J. Staiger[1,2,3,*]

[1] Department of Biological Sciences, Purdue University, West Lafayette, IN 47907
[2] Department of Botany and Plant Pathology, Purdue University, West Lafayette, IN 47907
[3] EMBRIO Institute, Purdue University, West Lafayette, IN 47907

[*] Address correspondence to: staiger@purdue.edu

ORCID IDs: 0000-0001-9629-7133 (L.X.); 0000-0002-2906-1566 (J.L.); 0000-0003-2321-1671 (C.J.S.).

Abstract

Precise control over how and where actin filaments are created in eukaryotic cells leads to the construction of unique cytoskeletal arrays with specific functions within a common cytoplasm. Actin filament nucleators are key players in this activity and include the conserved Actin-Related Protein 2/3 (Arp2/3) complex, that creates dendritic networks of branched filaments, as well as a large family of formins that typically generate long, unbranched filaments and bundles. In some eukaryotic cells, these nucleators compete for a common pool of actin monomers and loss of one favors the activity of the other. To test whether this is a common mechanism across kingdoms, we combined the ability to image single filament dynamics in living plant epidermal cells with genetic and/or small molecule inhibitor approaches to stably or acutely disrupt nucleator activity. We found that Arp2/3 mutants or acute CK-666 treatment markedly reduced the frequency of side-branched nucleation events as well as overall actin filament abundance. We also confirmed that plant formins contributed to side-branched filament nucleation *in vivo*. Surprisingly, simultaneous inhibition of both nucleators increased overall actin filament abundance and enhanced the frequency of *de novo* nucleation events. Collectively, these observations suggest that plant cells have a unique actin filament nucleation mechanism compared to yeast or animal cells.

Introduction

The actin cytoskeleton comprises a dynamic network of filaments that participates in a wide variety of cellular activities including plant cell expansion, mammalian cell migration, yeast cell division, general cell morphogenesis, and meiosis (Burke et al., 2014; Goley and Welch, 2006; Mathur et al., 2003b; Miller et al., 1989; Stürner et al., 2019; Szymanski et al., 1999). Plant cells rearrange their actin cytoskeleton organization on timescales of seconds to minutes in response to biotic or abiotic stimuli, which means the actin cytoskeleton organization is extremely dynamic but also precisely controlled (Henty-Ridilla et al., 2013b; Staiger et al., 2009). Regulation of the cytoskeleton involves more than a hundred actin-binding proteins (ABPs) that participate in filament nucleation, elongation, severing, and depolymerization. Nucleators initiate the formation of new actin filaments at a much faster rate than spontaneous nucleation from actin monomers and are therefore considered key regulators of array formation and actin dynamics (Kadzik et al., 2020; Rosenbloom et al., 2021). Previous *in vitro* studies demonstrate that the actin nucleation pathway utilizes both the actin-related-protein 2/3 (Arp2/3) complex and formins, two distinct actin filament nucleators with different specific activation mechanisms (Burke et al., 2014; Kovar, 2006; Paul and Pollard, 2008; Pollard, 2007; Suarez et al., 2015).

The Arp2/3 complex is a seven-subunit protein complex responsible for generating branched actin filaments and forming dendritic actin networks in eukaryotic cells (Beltzner and Pollard, 2008; Goley and Welch, 2006; Mullins et al., 1998; Pollard, 2007; Szymanski et al., 1999). The Arp2/3 complex undergoes a conformational change when it is activated by a collection of activators including nucleation promoting factors (NPFs), ATP, actin monomers, and pre-existing actin filaments. During Arp2/3 activation, the ARP2 and ARP3 subunits along with a recruited actin monomer can nucleate the polymerization of a new (daughter) filament, which grows from the side of a pre-existing (mother) actin filament with a characteristic 70° angle (Beltzner and Pollard, 2008; Dayel et al., 2001; Dayel and Mullins, 2004; Goley and Welch, 2006; Mullins et al., 1998; Pollard, 2007; Szymanski et al., 1999). This branched actin network structure is critical for many cellular processes such as exocytosis and endocytosis. Numerous *in vitro* studies have elucidated the Arp2/3 complex activation pathway and have mapped out its interactions with other ABPs. However, the exact role of the Arp2/3 complex in coordinating actin organization and filament dynamics *in vivo*, especially its coordination of the dynamic behavior of individual actin filaments, is not well understood.

Previous studies in *Saccharomyces cerevisiae* and *Schizosaccharomyces pombe* demonstrate that knockout mutations of single Arp2/3 complex subunits cause severe growth defects or even lethality (Cabrera et al., 2011; Winter et al., 1999). Knocking down the Arp2/3 complex with RNA interference (RNAi) in *Caenorhabditis elegans* is lethal, with defects of developing ventral closure (Roh-Johnson and Goldstein, 2009). So far, there is no indication that Arp2/3 mutants are lethal in mammals, but the RNAi-mediated knockout of *ARPC2* or *ARPC3* both result in defects on the asymmetric division and cytokinesis of mouse oocytes (Sun et al., 2013), which can further lead to failure of mouse embryo development. Furthermore, loss of Arp2/3 complex subunits causes developmental diseases in organs and tissues in these species (Di Nardo et al., 2005; Kahr et al., 2017; van der Kammen et al., 2017). In contrast, *Arabidopsis thaliana* plants with mutations in Arp2/3 complex subunits have relatively normal morphology and fertility; however, these Arp2/3 mutants have marked defects in epidermal cell morphology including distorted trichomes, cell-cell adhesion defects, and fewer lobes on leaf pavement cells (Harries et al., 2005; Le et al., 2003; Li et al., 2003; Mathur et al., 2003a; Szymanski et al., 1999; Yanagisawa et al., 2015). Recent research shows that plant Arp2/3 complex is also involved in auxin transport (García-González et al., 2020; Peng et al., 2017; Sahi et al., 2018), guard cell opening and closing (Jiang et al., 2012; Li et al., 2014), resistance to penetration-mediated infection by fungal pathogens (Qin et al., 2021), and possibly in autophagy (Wang et al., 2019; Wang et al., 2016). Many of these studies also reveal that *arp2/3* mutant cells have reduced actin filament abundance or misaligned actin bundles, which suggests that these functions of the Arp2/3 complex may be accomplished through regulating specific actin structures. In growing trichome branches, for example, the Arp2/3 complex generates a tip-localized actin filament array constrained by cortical microtubules that coordinates growth (Yanagisawa et al., 2018; Yanagisawa et al., 2015). During fungal invasion, the Arp2/3 complex localizes to the site of penetration peg attack in epidermal pavement cells and generates a large cortical actin filament patch necessary to suppress invasion (Qin et al., 2021). However, the molecular mechanisms by which the Arp2/3 complex coordinates the organization of cortical actin filament arrays in unstimulated cells or how it generates unique arrays in response to biotic and abiotic stress are poorly understood.

Another family of evolutionarily conserved actin filament nucleator are formins that typically generate long linear actin filaments that can bundle together to form actin cables (Kovar, 2006; Paul and Pollard, 2008; Pollard, 2007). These actin cables provide tracks for intracellular organelle/vesicle trafficking. Formins have two universally conserved formin-

homology domains, FH1 and FH2. The proline-rich FH1 domain allows formin to recruit profilin-bound actin to elongate actin filaments at the barbed ends. The FH2 domain, on the other hand, interacts with other regions within itself for autoinhibition or it can interact with the FH2 domain of another formin to form a dimer, which initiates the nucleation of linear actin filaments (Cheung and Wu, 2004; Cvrčková et al., 2000; Cvrčková et al., 2004; Deeks et al., 2002; Kovar, 2006; Michelot et al., 2006; Paul and Pollard, 2008; Pollard, 2007). There are 21 formin homologs in *Arabidopsis* and these are separated into two different phylogenetic subclasses (Cvrčková et al., 2000). Based on sequence prediction, Class I formins have a signal peptide and an N-terminal transmembrane domain that targets them to the plasma membrane. Class II formins are predicted to have more diverse domain structures (Cheung and Wu, 2004; Cvrčková et al., 2000; Cvrčková et al., 2004; Deeks et al., 2002; Michelot et al., 2006). In addition, these formin homologs can be categorized with respect to how they generate actin filaments. The processive formins remain attached to the actin filament barbed end and move processively as the filament elongates, whereas non-processive formins remain at the filament nucleation site (Cheung and Wu, 2004; Cvrčková et al., 2000; Cvrčková et al., 2004; Deeks et al., 2002; Michelot et al., 2006). Biochemical results reveal that a non-processive Class I formin, FORMIN1 (AFH1), attaches to the side of a pre-existing actin filament to nucleate new filaments, which suggests a far more complicated role of formins in plant cells than just generating linear filaments (Michelot et al., 2006). In addition, both *in vivo* and *in vitro* experiments showed that formins are critical for maintaining a normal actin structure as well as regulating polarized cell growth (Lan et al., 2018; Rosero et al., 2013; Vidali et al., 2009). However, the detailed molecular mechanism of how formins regulate actin structure and single actin filament dynamics in plant cells remains unclear.

Studies in fission yeast and animal cells indicate that the Arp2/3 complex and formins compete for a limited supply of actin monomers and this competition prevents excessive activity of one or the other, thereby allowing cells to generate different actin structures and dynamics by regulating the balance of activities between these two nucleators (Antkowiak et al., 2019; Chan et al., 2019; Davidson et al., 2018; Hotulainen and Lappalainen, 2006; Kadzik et al., 2020; Lomakin et al., 2015; Suarez et al., 2015). Furthermore, *in vitro* studies reveal that filaments with formin-mediated elongation grow faster than Arp2/3-nucleated ones (Funk et al., 2019; Michelot et al., 2013; Suarez et al., 2015; Vavylonis et al., 2006). However, the *in vivo* study of single actin filament dynamics is relatively hard to conduct in yeast and mammalian cells, because either the cells are too small or the actin arrays are too dense and filament lengths are

below the limits of resolution of light microscopy. Even though recent studies with advanced cryo-electron microscopy reveal detailed actin filament structures in mice neuronal cells and 3D organization analysis of cryo-electron tomography demonstrated the association of the Arp2/3 complex at actin filament branch junctions in *Dictyostelium* cells (Jasnin et al., 2019; Sartori-Rupp et al., 2019), these results do not directly demonstrate that the Arp2/3 complex generates side-branched filaments, and neither the cryo-electron microscopy nor cryo-electron tomography with animal cells can illustrate the real-time dynamic behavior of Arp2/3-made filaments *in vivo*.

Epidermal cells from dark-grown *Arabidopsis* hypocotyls are large in size and have relatively sparse actin arrays in the cortical cytoplasm, making this a powerful model system for quantitative analysis of single actin filament dynamics, especially when combined with high spatial and temporal resolution imaging approaches and genetically-encoded fluorescence reporters (Arieti and Staiger, 2020; Cai et al., 2014; Cao et al., 2016; Henty et al., 2011; Henty-Ridilla et al., 2013a; Staiger et al., 2009). Previous work demonstrates a remarkably high rate of new filament construction, rapid growth at filament ends, and disassembly by prolific severing activity in a mechanism termed “stochastic dynamics” (Staiger et al., 2009). The ability to observe both actin filament architecture and activities of single filaments in living cells allows direct visualization of the effect of disruption of actin nucleators on filament activities *in vivo* (Cao et al., 2016). A recent study in *Arabidopsis* shows that actin arrays in cotyledon epidermal pavement cells are slightly more dense and the extent of bundling is unchanged when either a Class I formin, AFH1, or the Arp2/3 subunit, ARPC5, are genetically down-regulated; however, single filament dynamics or nucleation events were not evaluated directly (Cifrová et al., 2020). The authors propose that the Arp2/3 complex and formins in plants may have complementary roles to overcome the loss of one or the other. Nevertheless, the underlying mechanism of filament nucleation and the nature of the actin arrays that each nucleation factor constructs remain to be fully elucidated.

In this study, we test the hypothesis that the plant Arp2/3 complex mediates the nucleation of side-branched filaments *in vivo* but does not facilitate filament elongation directly. We used both genetic and pharmacological approaches to disrupt Arp2/3 complex activity in plant cells. With quantitative live-cell imaging at single filament resolution, we demonstrated that the Arp2/3 complex is responsible for the nucleation of side-branched filaments. We also characterized the difference between the Arp2/3 complex and formins with respect to the dynamic behaviors of the filaments they generate and evaluated the consequence of losing both

classes of filament nucleator on actin organization and dynamics. Surprisingly, living plant cells deficient for two classes of nucleator generate comparatively normal and dynamic actin arrays by an apparent *de novo* filament nucleation mechanism.

Results

Arabidopsis plants have defects in general growth and epidermal cell morphology when deficient for the Arp2/3 complex

Previous studies of Arp2/3 complex mutants reveal defects in *Arabidopsis* epidermal cell growth and morphology (Cifrová et al., 2020; Facette et al., 2015; Harries et al., 2005; Le et al., 2003; Li et al., 2003; Mathur et al., 2003b; Szymanski et al., 1999; Yanagisawa et al., 2015). Here, we acquired a homozygous T-DNA insertion mutant for *ARP2*, *arp2-1* (or *wrm1-2*; SALK_003448), and a point mutation of *ARPC2*, *arpc2* (or *dis2-1*; (El-Assal et al., 2004), and confirmed the cell and organ growth phenotypes. We confirmed that both *arp2-1* and *arpc2* mutant plants had adhesion defects at end walls of hypocotyl epidermal cells and severely distorted leaf trichomes when compared to wild-type siblings (Fig. 1 A). In addition, hypocotyls of *arp2-1* and *arpc2* were significantly shorter than wild-type siblings at the same time points (Fig. 1, B and C). To test whether hypocotyl growth defects resulted from defects in cell expansion, we examined epidermal cell length and found that cells in all regions of etiolated *arp2/3* hypocotyls were significantly shorter compared to wild-type hypocotyls; however, cell widths were not affected (Fig. 1, D and E). Similar results for root growth were observed in light-grown seedlings (Fig. 1, F and G). These results confirm that the Arp2/3 complex plays a role in axial cell expansion in both dark-grown hypocotyls and light-grown roots of *Arabidopsis*.

Actin filament abundance and bundling are reduced in *arp2/3* mutants

To assess the influence of the Arp2/3 complex on cortical actin cytoskeletal organization, we compared images of epidermal cells from the apical region of 5-day-old etiolated wild-type, *arp2-1,* and *arpc2* hypocotyls collected by variable-angle epifluorescence microscopy (VAEM) (Staiger et al., 2009). Homozygous mutant and isogenic wild-type sibling lines that express the actin reporter, green fluorescent protein (GFP) fused with FIMBRIN1 actin-binding domain 2 or GFP-fABD2 (Sheahan et al., 2004) were prepared by crossing, allowing observation and measurement of the organization and filament dynamics of the actin cytoskeleton (Staiger et al., 2009). The actin array structure in *arp2-1* and *arpc2* cells had fewer, thinner, and more scattered filaments compared to corresponding wild-type cells (Fig. 2 A). To compare these

differences quantitively, we used *density*, *skewness, angle*, and *parallelness* as four key parameters established previously for standardized descriptions of actin cytoskeleton array organization in living cells (Arieti and Staiger, 2020; Cai et al., 2014; Cao et al., 2016; Henty et al., 2011; Higaki et al., 2010; Li et al., 2012; Ueda et al., 2010). Density measures the percentage of occupancy of actin filaments, skewness defines the extent of bundling of actin filaments, and angle and parallelness describe how filaments orient relative to the longitudinal axis of the cell or each other, respectively. Actin density in *arp2-1* and *arpc2* cells was significantly decreased compared to the respective wild-type sibling cells (Fig. 2 B), and the extent of filament bundling was significantly reduced as well (Fig. 2 C). The average angle of filament arrays was not significantly different between *arp2-1*, *arpc2,* and wild-type sibling cells (Fig. 2 D). The population distribution of filament parallelness in *arp2-1* and *arpc2* was left-skewed compared to that in the wild type, indicating that filaments were more parallel to each other in *arp2/3* mutant cells; however, the mean values were not significantly different between any of these genotypes (Fig. 2 E). These results demonstrate that the Arp2/3 complex contributes to the generation of both individual filaments and filament bundles and is necessary for maintaining the normal architecture of the cortical actin cytoskeleton in epidermal cells.

The Arp2/3 complex plays a significant role in filament nucleation and generation of side-branched filaments

To investigate how the Arp2/3 complex participates in actin filament nucleation, we measured single actin filament formation and dynamics in wild-type and *arp2/3* mutant cells by collecting time-lapse movies from the apical regions of 5-day-old dark-grown hypocotyls with VAEM. The sparse nature of the cortical actin array in plant epidermal cells and the high spatial and temporal resolution afforded by VAEM allowed us to visualize (Fig. 3 A) and quantify individual nucleation events by a previously described assay (Cao et al., 2016). Briefly, we counted all new or regrowing filaments identified in multiple 400 μm^2 regions of interest (ROI) within a cell during a 100-s time-lapse movie. The nucleation frequency was normalized to the average filament number within the ROI to minimize the influence of filament abundance differences between ROIs and genotypes. The overall nucleation frequency in *arp2-1* cells (0.36 ± 0.03 events/filament/min) was significantly decreased compared to wild-type cells (0.61 ± 0.03 events/filament/min) (Fig. 3 B; Video 1; and Video 2), and coincided with our observation that loss of function of the Arp2/3 complex resulted in a significant reduction in filament abundance (Fig. 2 B). Similar reductions in overall nucleation frequency were also observed for *arpc2* compared to wild-type cells (Fig. S1 A). Next, we classified nucleation events into three different

subpopulations based on filament origin: *de novo* from the cytoplasm; from the side of a pre-existing filament or bundle; or, from the end of a pre-existing filament (Fig. 3 A; Video 3 to 5) (Cao et al., 2016; Henty-Ridilla et al., 2013a; Staiger et al., 2009). Only the side-branched nucleation frequency was significantly decreased in *arp2-1* and *arpc2* cells compared to the respective wild-type sibling cells (Fig. 3 C; Video 1; Video 2; and Fig. S1 A). Side-branched nucleation events contribute about half of all new filament origins and these were reduced by 60–70% in the *arp2/3* mutants.

To understand how the Arp2/3 complex influences the dynamics of actin filaments, we tracked many dozens of individual filaments from their first appearance to complete disappearance and measured several parameters that were previously established to describe actin filament turnover (Fig. 4 A; Table 1; Video 6 and 7). Compared to wild type, the population distribution of actin filament elongation rate in *arp2-1* cells was more left-skewed, and the average filament elongation rate was also higher (Fig. 4 B; Table 1), indicating that actin filaments were growing significantly faster in *arp2-1* cells. It is also obvious that there were two or three distinct populations of filament elongation rates with peaks at 0.75 – 1.25, 2.0 – 2.25, and > 3 μm/s with the latter two categories becoming more prevalent in *arp2-1* cells (Fig. 4 B). Similar differences in overall elongation rate and fast-growing filament populations were observed in *arpc2* (Table S1 and Fig. S1 E). Filaments in both *arp2-1* and *arpc2* mutant cells also had significantly longer filament length and lifetimes than the ones in wild-type sibling cells (Table 1 and Table S1).

Previous *in vitro* data suggest that filament ends generated by the Arp2/3 complex and formins have different elongation rates; many formins are processive assembly motors that use profilin-actin to add monomers to growing filaments (Akin and Mullins, 2008; Kovar et al., 2003; Romero et al., 2004). To test whether dynamic properties of filaments with different nucleation patterns are distinct from each other, we measured the full suite of dynamic parameters for each population. We found that side-branched filaments in *arp2-1* cells were significantly longer (Fig. 4 C) and filament lifetime was prolonged (Fig. 4 D) compared to the side-branched filaments in wild-type cells; in addition, the filament severing frequency was slightly reduced in *arp2-1* cells (Fig. 4 E). These dynamic differences between side-branched filaments in *arpc2* mutant and wild-type sibling cells were conserved (Fig. S1).

Collectively, these data demonstrate that the Arp2/3 complex is responsible for generating new filaments from the side of pre-existing filaments and is necessary for cells to

maintain the homeostatic actin cytoskeleton architecture. Moreover, Arp2/3-nucleated filaments have distinct dynamic properties compared with those generated *de novo* or from the end of a pre-existing filament; in particular, they grow slower and are shorter, and have reduced filament lifetimes.

The small molecule inhibitor CK-666 phenocopies actin-based defects in *arp2* and *arpc2* mutants

Recent studies show that CK-666, a small molecule inhibitor of the Arp2/3 complex that is effective on yeast and animal cells (Hetrick et al., 2013; Nolen et al., 2009), phenocopies the effects of *arp2/3* mutants on tomato pollen tube growth (Liu et al., 2020) and *Arabidopsis* sperm nuclear migration (Ali et al., 2020), both of which depend upon the actin cytoskeleton. Although the latter studies did not directly demonstrate the effects of CK-666 on actin structure or filament nucleation, they do suggest that CK-666 could be a potential Arp2/3 complex inhibitor in plant cells. We hypothesized that applying CK-666 to wild-type *Arabidopsis* cells would inhibit the Arp2/3 complex activity and mimic the *arp2/3* mutant phenotypes described above. To test the effects of this Arp2/3 complex inhibitor, we applied a dose series of CK-666 (0, 1, 5, 10, 50, and 100 μM) for 5 min and collected snapshots of epidermal cells from the apical region of treated hypocotyls. Compared to the mock treatment (0 μM), CK-666 started to have a significant reduction on both filament density and the extent of bundling at 5 μM and reached its maximum effect at 10–50 μM (Fig. S2, A, B, and C). A time-course (0, 5, 10, 30, and 60 min) of 10 μM CK-666 treatment showed that 5 min was sufficient to alter actin array organization (Fig. S2, A, D, and E). Finally, cells were able to recover normal actin array architecture from a 5 min, 10 μM CK-666 application after a 30-min wash out (Fig. S2, A, F, and G).

To further examine whether CK-666 phenocopies *arp2/3* mutants, we treated 5-day-old dark-grown hypocotyls of wild type and *arp2-1* with either mock solution or 10 μM CK-666 for 5 min and measured actin organization and single filament dynamics. Compared to mock-treated wild-type cells, the CK-666-treated wild-type cells had significantly decreased filament abundance (Fig. 5, A and B), extent of filament bundling (Fig. 5, A and C), as well as overall nucleation frequency (Fig. 3 B), and these changes mirrored actin organization in mock-treated *arp2-1* cells. Moreover, treatment of *arp2-1* with CK-666 showed no differences in terms of filament organization or dynamics compared to *arp2-1* alone (Fig. 5, A to D; and Fig. 3 B). CK-666 treatment also potently suppressed side-branched filament nucleation in wild-type cells, but not end or *de novo* filament origins (Fig. 3 C; Video 1 and 8), thereby fully phenocopying the effects of *arp2-1*. Finally, treatment of *arp2-1* with CK-666 did not further reduce filament side-

branch nucleation events, indicating that its likely mode of action is to inhibit daughter filament formation from a mother filament by the Arp2/3 complex (Fig. 3 C; Video 8 and 9).

When we compared CK-666 treatment of *arpc2* with its wild-type siblings, there were similar changes in actin architecture and filament nucleation frequency (Figs. S1 and S3). Therefore, we validated CK-666 as a small molecule inhibitor that targets the Arp2/3 complex and demonstrate its utility as an acute but reversible inhibitor for studying the Arp2/3 complex in plant systems.

The Arp2/3 complex and formins are both capable of nucleating side-branched filaments

Our previous work showed that profilin-bound actin monomers favor formin-mediated fast actin filament elongation at rates > 2 μm/s (Cao et al., 2016), and the data above suggest that Arp2/3-nucleated filament barbed ends elongated at intermediate rates of 1.25 – 1.5 μm/s (Fig. 4 B and Fig. S1 E). We previously demonstrated the effectiveness of Small Molecule Inhibitor of Formin Homology 2 (SMIFH2) in *Arabidopsis* (Cao et al., 2016). Actin array organization and nucleation frequency were significantly reduced when wild-type cells were treated with 25 μM SMIFH2 for 5 min (Cao et al., 2016), and similar results were obtained here (Fig. 6; Fig. 7; and Video 1 and 10).

To test whether filament arrays generated by these two nucleators are distinct, we genetically- and/or chemically-inhibited the Arp2/3 complex and formins. Both Arp2/3-inhibited (mock-treated *arp2-1* or *arpc2)* or formin-inhibited (SMIFH2-treated wild type) cells had a significant decrease in actin filament abundance compared to mock-treated wild type (Fig. 6, A, B; and Fig. S4, A, B). However, SMIFH2 treatment of wild type led to only a modest reduction in the extent of bundling (Fig. 6 C and Fig. S4 C), whereas *arp2/3* mutants had a substantial reduction in bundling. Moreover, filaments were more parallel to each other when the Arp2/3 complex was inhibited compared to the ones with formin activity suppressed (Fig. 6 D and Fig. S4 D). Thus, both the Arp2/3 complex and formins are required to generate dense arrays of individual actin filaments, however, their contributions to actin bundling and filament parallelness are distinct.

To test whether filament dynamics or types and extent of filament nucleation are distinctly due to the Arp2/3 complex or formins, we examined single filament dynamics in genetically- and/or chemically- inhibited material. The nucleation frequency of both total and side-branching filaments was significantly decreased in both Arp2/3-inhibited (mock-treated

arp2-1) and formin-inhibited (SMIFH2-treated wild type) cells compared to wild type (Fig. 7 A; Video 2 and 10), and the nucleation frequency of side-branched filaments in Arp2/3-inhibited cells (0.082 ± 0.022 events/filament/min) was ~50% less than in formin-inhibited cells (0.16 ± 0.013 events/filament/min). However, the nucleation frequency due to *de novo* filament origins was not influenced when either the Arp2/3 complex or formin was suppressed (Fig. 7 A). The average filament elongation rate in Arp2/3-inhibited cells (1.85 ± 0.10 μm/s) was also significantly higher than the rate in formin-inhibited cells (1.57 ± 0.11 μm/s) or in wild-type cells (1.72 ± 0.10 μm/s). In addition, the population distribution of filament elongation rates in Arp2/3-inhibited cells was significantly left-skewed (peak value at 2.0 – 2.25 μm/s) compared to wild type (peak value at 1.25 – 1.5 μm/s), whereas formin-inhibited cells lost a large portion of filaments elongating at 2.0 – 2.25 μm/s but the distribution had a prominent peak at 1.0 – 1.5 μm/s (Fig. 7 E). We did not, however, observe any significant difference in filament length, lifetime, or filament severing frequency when parameters of side-branched filaments in Arp2/3-inhibited cells and formin-inhibited cells were compared (Fig. 7, B to D). Again, we found similar results in both actin architecture (Fig. S4) and single filament dynamics (Fig. S5) when *arpc2* and its wild-type sibling treated with mock solution or SMIFH2 were compared. These data indicated that both the Arp2/3 complex and formin predominantly generate side-branched actin filaments and formin-nucleated filaments elongate faster than Arp2/3-nucleated ones.

To test whether SMIFH2 has off-target inhibition of myosin superfamily members as reported in *Drosophila* (Nishimura et al., 2021), we evaluated the influence of SMIFH2 (and CK-666) on the activity of myosin XIK, the major myosin isoform mediating the delivery, vesicle tethering, and exocytosis of secretory vesicles in *Arabidopsis* cells (Zhang et al., 2021). We found that neither SMIFH2 or CK-666 treatment reduced the motility of myosin XIK-YFP compared to pentabromopseudilin (PBP), an effective myosin inhibitor in plant cells (Fig. S6, B to D) (Zhang et al., 2019). In addition, we also measured the filament convolutedness and the rate of change of convolutedness of actin filaments, which are parameters describing the buckling and straightening of filaments (Cai et al., 2014; Staiger et al., 2009). Filament convolutedness and rate of change of convolutedness were significantly decreased with SMIFH2 and PBP treatment, but unchanged by CK-666, indicating that SMIFH2 does indeed alter filament buckling and straightening (Table S2 and Fig. S6 A). These data suggest that SMIFH2 may not have off-target effect on activities of myosin based on the lack of effect on motility of YFP-XIK, but it is still possible that SMIFH2 targets other myosin isoforms besides myosin XIK. Although the inhibition of filament buckling and straightening could indicate an off-

target effect of SMIFH2 on myosin XI, it seems equally likely that filament buckling is caused by processive assembly of actin filaments by plant formins (Table S2).

Combined genetic and chemical inhibition of Arp2/3 and formins increases spontaneous filament nucleation and overall actin filament abundance

Using chemical and genetic tools to suppress the activity of both the Arp2/3 complex and formin simultaneously, we applied SMIFH2 to *arp2-1 or arpc2* mutant cells, or treated wild-type cells with a combination of SMIFH2 and CK-666, to test whether different nucleators cooperate or compete to form actin filament arrays in plant cells. Since the Arp2/3 complex and formin are, so far, the only two actin filament nucleators identified in plant cells, we predicted that inhibiting both the Arp2/3 complex and formin should severely suppress actin filament nucleation activities and significantly reduce filament abundance. Surprisingly, in *arp2-1* cells treated with SMIFH2, actin filament abundance was dramatically increased compared to cells with normal Arp2/3 complex and formin activities or with only one nucleator inhibited (Fig. 6, A and B). Notably, SMIFH2-treated *arp2-1* cells had a marked abundance of short, single actin filaments in the cortical array (Fig. 6 A). Unlike actin array density, the extent of actin filament bundling was not restored to wild-type levels when both the Arp2/3 complex and formins were inhibited; indeed, overall bundling was lower in SMIFH2-treated *arp2-1* compared to *arp2-1* alone (Fig. 6 C). In addition to increased filament abundance, total filament nucleation frequency was significantly increased when both the Arp2/3 complex and formin activities were reduced, and a 2.5-fold enhancement of *de novo* filament origins was responsible for this increase (Fig. 7 A and Video 11). However, the lengths of filaments generated *de novo* or from the side-branching nucleation events were both significantly reduced in SMIFH2-treated *arp2-1* cells compared to other treatments and genotypes (Fig. 7 B). Finally, we also observed similar phenotypes in both actin architecture and filament dynamics when we applied SMIFH2 to *arpc2* (Fig. S5) or applied both CK-666 and SMIFH2 to wild type (Fig. 8). These results indicate that a marked increase in *de novo* filament nucleation results when both the Arp2/3 complex and formins are inhibited in plant cells.

Discussion

In this study, we utilized a combination of genetic mutations or small molecule inhibitors along with high spatiotemporal resolution fluorescence microscopy to demonstrate, for the first time, that the Arp2/3 complex nucleates side-branched actin filaments in *Arabidopsis thaliana* epidermal cells. We found that the Arp2/3 complex mutants, *arp2-1* and *arpc2*, had a dramatically reduced overall abundance of actin filaments in the cortical array, a reduction in the extent of filament bundles, and a significantly decreased frequency of side-branched nucleation events. In addition, acute treatment of wild-type plants with CK-666 phenocopied the actin-based defects observed in *arp2/3* mutants, whereas applying CK-666 to *arp2/3* mutants did not have any additional effect on overall actin structure or filament dynamics. Thus, we confirmed that these actin-based defects correlated with the loss of functional Arp2/3 complex and also established that CK-666 is an effective tool for inhibition of the Arp2/3 complex in plant cells. Through experiments comparing genetic and chemical inhibition of the Arp2/3 complex or formins, we observed that both proteins were capable of nucleating side-branched actin filaments, but that Arp2/3-nucleated filaments grew slower and were shorter than formin-nucleated ones. Surprisingly, simultaneous inhibition of both the Arp2/3 complex and formins led to an increase in actin filament abundance and dramatically promoted *de novo* nucleation events. These observations indicate that the regulatory mechanisms for actin filament nucleation in plant cells are different from yeast and animal cells.

The Arp2/3 complex is a major nucleator of side-branched actin filaments in *Arabidopsis* epidermal cells

Nucleation is the rate-limiting step for actin filament formation *in vitro* and depends on the availability of actin monomers and is suppressed by profilin (Michelot et al., 2005; Pollard et al., 2000; Sept and McCammon, 2001). In cells, filament nucleation is also accepted as a key step in generating new actin arrays for various cellular activities, such as driving cell migration and powering organelle movements. Biochemical studies demonstrate that the Arp2/3 complex and formins use different molecular mechanisms to overcome the rate-limiting step for filament formation and they typically create different types of actin structure. After creating a nucleus, representing the first three subunits of a two-stranded helix, and initiating filament elongation, the Arp2/3 complex remains attached at the nucleation site and the filament barbed end is free

for the addition of actin monomers, profilin-actin, or capping protein (Amann and Pollard, 2001; Fujiwara et al., 2002; Ichetovkin et al., 2002; Mullins et al., 1998; Rouiller et al., 2008). In contrast, formins overcome the suppression of nucleus formation by directly interacting with profilin and actin through FH1 and FH2 domains. After the nucleation step, many formins remain associated at the barbed end of actin filaments and processively facilitate filament growth through the addition of profilin-actin. This allows formin-associated filaments to grow much faster and longer compared to filaments with free barbed ends that are typically bound by heterodimeric capping protein (CP) soon after initiation. The occupation of formin at the barbed end can also prevent CP from binding and limiting subunit addition or loss (Kovar, 2006; Kovar and Pollard, 2004; Romero et al., 2004). Based on these observations, the conventional model of actin nucleation posits that formin mediates long, unbranched filaments with a fast filament elongation rate whereas the Arp2/3 complex nucleates short, branched actin networks with a slower growth rate.

The Arp2/3 complex has been accepted as the major nucleator of side-branched actin filaments in yeast and animal cells (Amann and Pollard, 2001; Fujiwara et al., 2002; Ichetovkin et al., 2002; Mullins et al., 1998; Rouiller et al., 2008). Even though the Arp2/3 complex is also shown to be critical for cells to maintain their homeostatic actin organization and is required for epidermal cell morphogenesis, defense against fungal penetration, auxin transportation, and other cellular activities, little is known about the exact function of plant Arp2/3 complex in terms of its contribution in regulating actin filament dynamics. In this study, we characterized the function of the Arp2/3 complex in regulating the organization of the cortical actin array as well as single actin filament dynamics in living *Arabidopsis* cells. Epidermal cells of dark-grown hypocotyls with genetically- or chemically-inhibited Arp2/3 complex showed a quantifiable decrease in both actin filament abundance and extent of filament bundling, and, more importantly, there was a significantly reduced nucleation frequency of side-branched actin filaments. Branched filament formation represents more than half of all nucleation events in the cortical actin array of hypocotyl epidermal cells and these are reduced by 60–70% when the Arp2/3 complex is inhibited chemically or genetically. These results suggest that the Arp2/3 complex is a major nucleator of side-branched actin filaments in plant cells. Our data also provide the first live cell view of the formation of branched actin filaments by active Arp2/3 complex at single filament resolution. Furthermore, our results reveal that there are at least two populations of filaments with different dynamic properties, likely due to different filament growth mechanisms and/or availability of filament barbed ends for monomer addition, that contribute to

the organization of the plant actin cortical array in epidermal cells. By examining filament elongation rate frequencies when formin activity is suppressed, or even when both the Arp2/3 complex and formins are inhibited, filaments with elongation rates of 1 – 1.25 μm/s predominate. We expect this represents the population of filaments with free barbed ends extending by monomer addition and is consistent with the *in vitro* mechanism of branched filament nucleation by the Arp2/3 complex.

The Arp2/3 complex and formins both mediate side-branched filament nucleation but generate filaments with unique dynamic properties

Previous *in vivo* results with the fission and budding yeasts, *Schizosaccharomyces pombe* and *Saccharomyces cerevisiae*, as well as mammalian cells reveal a competition between the Arp2/3 complex and formin for a limited pool of actin monomers; consequently, formin-mediated long filament bundles dominate when the Arp2/3 complex is inhibited, whereas an increased abundance of actin patches created by the Arp2/3 complex are prominent when formin is down-regulated (Antkowiak et al., 2019; Burke et al., 2014; Chan et al., 2019; Davidson et al., 2018; Hotulainen and Lappalainen, 2006; Kadzik et al., 2020; Lomakin et al., 2015; Suarez et al., 2015). Plant cells, by contrast, appear to show cooperation between these two nucleators rather than a competition to build distinct actin arrays. The cortical cytoplasm of epidermal cells contains a dynamic actin array that is rather disordered and comprises comingled actin filament bundles and individual actin filaments (Staiger et al., 2009; Smertenko et al., 2010). Evidence for actin patches or dense dendritic actin networks is limited to certain cell types, such as guard mother cells (Facette et al., 2015), the apex of trichomes (Yanagisawa et al., 2015), or at focal sites elicited by pathogen attack (Hardham et al., 2007; Qin et al., 2021). Our results revealed that the density of actin filaments in the cortical array, extent of filament bundling, as well as filament nucleation frequency all decreased when either the Arp2/3 complex or formins were inhibited, suggesting that formins were not able to maintain the actin abundance at normal levels when the Arp2/3 complex was genetically- or chemically- inhibited, and the Arp2/3 complex also failed to do so when formins were inhibited. These results indicate that plant cells may have a different actin regulatory mechanism for constructing actin filament arrays compared to yeast or some animal cells. Our results are consistent with a previous report showing partial cooperation between plant filament nucleation mechanisms in *Arabidopsis* cotyledon epidermal cells, but the consequences of losing either class of nucleator was markedly different (Cifrová et al., 2020). That study showed a minor increase in actin filament

density in either the formin *fh1* mutant or the *arpc5* mutant (Cifrová et al., 2020), rather than the prominent decreases observed here. These differences could be due to the use of different actin filament reporters (LifeAct versus fABD2), different developmental state and organ for examining epidermal cells (cotyledons versus dark-grown hypocotyls), or the result of compensation from genetic loss of one formin isoform versus acute treatment with a chemical inhibitor. The previous results are not obviously consistent with the loss of nucleation machinery; however, individual filament dynamics were not examined to test whether nucleation activity or filament formation was suppressed by the loss of the Arp2/3 complex or AFH1.

Our results showed that both the Arp2/3 complex and formins are responsible for generating side-branched filaments because the inhibition of either one lead to significantly reduction in side-branched filament nucleation and did not promote the other two types of filament nucleation. These results also suggest that the Arp2/3 complex and formins are not competing for actin monomers for filament nucleation. Based on the total actin concentrations and the ratio of F- to total actin in both maize pollen and poppy pollen, the estimated actin monomer pool in *Arabidopsis* hypocotyl cells is relatively large and most monomers are likely to be in a profilin-actin complex (Staiger et al., 2010); therefore, the Arp2/3 complex and formins may not have to compete for excess supply of actin monomers in plant cells. Here, if we assume that 1.25 μm/s is the rate of addition of monomers to free barbed ends, that the association rate constant for plant actin is similar to ATP-loaded rabbit skeletal muscle α-actin ($k_+ = 11.6\ \mu M^{-1}\ s^{-1}$) and that a micron of actin filament comprises 370 subunits (Pollard et al., 2000), then we estimate the available monomer pool to be 40 μM in hypocotyl epidermal cells using the equation: [G-actin] = rate/k_+. In addition, even though both the Arp2/3 complex and formins generate side-branched actin filaments, these filaments have markedly different properties. We found that formin-nucleated filaments grew significantly faster at rates of 2 – 2.25 μm/s, with another small subpopulation growing at rates > 3 μm/s, compared to Arp2/3-generated ones. The different properties of filament barbed ends as well as a large pool of monomers perhaps buffered with profilin, may facilitate the fast-growing filaments nucleated by side-branching as previously found in *Arabidopsis* cells (Cao et al., 2016), and is consistent with previous *in vitro* results (Funk et al., 2019; Michelot et al., 2013; Suarez et al., 2015; Vavylonis et al., 2006).

If using the conventional model for how formins generate new actin filaments, we should expect that plant processive formins not only generate growing filaments from the side of a

mother filament but also remain attached to the barbed end of the new filament to facilitate the addition of profilin-actin to the growing ends, which results in faster and longer side-branched filaments compared to Arp2/3-nucleated ones. However, previous *in vitro* data showed that the formin AtFH1 nucleates actin filaments but remains associated at the pointed end and does not compete with capping protein for filament barbed ends, indicating it is non-processive and associates with the side of filaments after nucleation (Michelot et al., 2006). Further, SMIFH2 application in our studies reduced nucleation frequency but did not reduce the filament length of side-branched filaments compared to the mock treatment. Both *in vitro* and *in vivo* results suggest that non-processive formins in plant cells may have a weak interaction with filament barbed ends so that these formins move away from the end of the filament to its side to generate a new side-branched filament instead of occupying the barbed end and facilitating filament elongation. However, another *in vitro* analysis showed that the processive formin, AtFH14, promotes *de novo* filament growth via the association with profilin (Zhang et al., 2016), and there are 21 FORMIN homologs in *Arabidopsis* (Blanchoin and Michelot, 2012; Cvrčková, 2013; Cvrčková et al., 2004). All these results suggest that plant formins that nucleate side-branched filaments may have distinct molecular properties to formins that nucleate *de novo* filament formation or formins found in yeast or animal cells. It is important to note that SMIFH2 is capable of suppressing the nucleation activity of the non-processive AFH1 *in vitro* (Cao et al., 2016), so it seems probable that at least one class of plant formins is being suppressed in inhibitor-treated cells.

Since SMIFH2 shows off-target inhibition of members of the myosin superfamily (Nishimura et al., 2021), we are compelled to critically evaluate the effects of SMIFH2 treatment of plant cells. Although our data showed that SMIFH2 treatment did not influence the motility of myosin XIK, it did significantly reduce filament convolutedness and the rate of change of convolutedness of actin filaments, suggesting that SMIFH2 alters filament buckling and straightening. However, the change of filament buckling could be the consequence of different filament growth rates and processive elongation by formins (Cai et al., 2014; Cao et al., 2016; Staiger et al., 2009). Even though a recent *in vitro* study reveals that SMIFH2 is a pan-inhibitor for all human formins (Orman et al., 2022), we should not exclude the possibility that SMIFH2 can only inhibit a subset of plant formin homologs, perhaps only the non-processive ones. These facts suggest that we need to be cautious about making conclusions concerning formin *in vivo* functions since this conclusion relies solely on SMIFH2 inhibition. Further genetic and biochemical analyses should be designed to dissect the interaction between SMIFH2 and

different formin homologs in order to determine the specificity of this chemical inhibitor on plant formins.

Simultaneous inhibition of the Arp2/3 complex and formins promotes *de novo* nucleation events

When we combined genetic and chemical methods to down-regulate the Arp2/3 complex and formins simultaneously, surprisingly, the frequency of actin filament nucleation was significantly enhanced, with *de novo* nucleation events appearing to be the exclusive contributor to this enhancement. A similar experiment in *Arabidopsis* cotyledon epidermal pavement cells with the *fh1 arpc5* double mutant also showed a minor increase in actin density (Cifrová et al., 2020). The Arp2/3 complex and formins are, to date, the only two *bona fide* actin filament nucleators in plant cells (Blanchoin and Staiger, 2010; Vaškovičová et al., 2013; Yanagisawa et al., 2013). Theoretically, when both the Arp2/3 complex and formins are inhibited, the concentration of free actin monomers is predicted to increase but the ratio of F- to G-actin and the proportion of profilin-actin in the monomer pool should both decrease. It is possible that these changes in the actin monomer pool could increase the nucleation rate of spontaneous filament formation thereby enhancing the total frequency of *de novo* nucleation events. In support of this model, disruption of AtPRF1 led to an increase in *de novo* nucleation events and a decrease in side-branched events (Cao et al., 2016). Here, the amount of *de novo* filaments was dramatically increased when both the Arp2/3 complex and formins were inhibited but the average length was significantly shorter compared to the ones generated from other origins. This observation fits the previous biochemical study that showed the relationship between the average length of filaments grown *de novo* and the number of these filaments fits an exponential distribution instead of a Gaussian distribution (Burlacu and Borejdo, 1992).

A previous study with fission yeast reveals that inhibiting the Arp2/3 complex with CK-666 in the formin double mutant *cdc12-112 for3⊿* depletes most of the actin bundles but not the actin patches (Burke et al., 2014). The resulting actin arrays were rather static, however, unlike the dynamic arrays after simultaneous inhibition of the Arp2/3 complex and formins found in plant cells. The different actin dynamic behaviors between yeast and plant cells when both the Arp2/3 complex and formins are both inhibited suggests a possible unique filament nucleation mechanism in plant cells that can overcome the requirement of these two major nucleators. However, considering the fact that SMIFH2 treatment only inhibits the side-branched filament nucleation in *Arabidopsis*, we cannot rule out the possibility that our double inhibition treatment

inhibited only nucleators for generating side-branched filaments. In this case, the *de novo* filament nucleation by SMIFH2-insensitive formin homologs might become significantly enhanced. In addition, it is also possible that there is an unknown actin nucleator in *Arabidopsis* that facilitates *de novo* filament nucleation when the major side-branched filament nucleators are inhibited. This unknown nucleator may be inactive when the Arp2/3 complex and formins are present, or it may have a much lower binding affinity for actin monomers compared to the Arp2/3 complex and formins.

Another unexpected result from inhibiting the Arp2/3 complex or formins is that the extent of actin filament bundling decreased when either nucleator was down-regulated, suggesting that side-branched actin filaments generated by both the Arp2/3 complex and formins are assembled into actin bundles. In addition, the down regulation of the Arp2/3 complex has a greater effect on the extent of filament bundling compared to formin inhibition, which may indicate that filaments generated by the Arp2/3 complex contribute more to construction of actin bundles than the ones generated by formins.

In conclusion, our results provide direct evidence to demonstrate that the Arp2/3 complex nucleates side-branched actin filaments in living plant cells. These studies also confirm that some formin homologs generate side-branched actin filaments in plant cells, which is a unique actin filament nucleation mechanism compared to yeast or animal cells. Moreover, we find that Arp2/3- and formin-nucleated filaments have distinct dynamic properties, which can be applied to future studies about how cells coordinate these two nucleators to regulate the actin structure and dynamics for different cellular activities. The dual-inhibition of both the Arp2/3 complex and formin surprisingly caused an enhanced *de novo* filament nucleation, which raises the possibility for a unique actin nucleation mechanism to generate dynamic cortical actin arrays in plant cells.

Material and Methods

Plant Material and Growth Conditions

All Arabidopsis (*Arabidopsis thaliana*) plants in this study were in Columbia-0 (Col-0) background. The *ARP2* T-DNA insertion line, *arp2-1* (SALK_003448), was obtained from the

Arabidopsis Biological Resource Center (Ohio State University) and the *ARPC2* point mutation line, *arpc2* (G1217A), was kindly provided by Dan Szymanski (Purdue University). Both *arp2-1* and *arpc2* mutant lines were crossed to wild-type (Col-0) expressing the GFP-fABD2 reporter (Sheahan et al., 2004; Staiger et al., 2009) and homozygous mutants and corresponding wild-type siblings were recovered from F2 populations.

Seeds were surface sterilized and stratified at 4°C for 3 days on plates comprising half-strength Murashige and Skoog (MS) medium supplemented with 1% (w/v) sucrose and 1% (w/v) agar. For dark-grown hypocotyl growth, seedlings were grown in continuous darkness after exposing the plates to light for 4 h. For light-grown root growth, seeds were grown vertically on plates comprising half-strength MS medium supplemented with 0% (w/v) sucrose and 0.6% (w/v) agar under long day conditions (16 h light/8h dark) at 21°C.

A double-blinded experimental design was used for all phenotypic analysis. All image measurements were performed with Image J (National Institutes of Health, Bethesda, MD. http://rsb.info.nih. gov/ij/).

Drug Treatments

For short-term live cell treatments, individual seedlings were treated for 5 min in inhibitor solution in 6-well plates in the dark prior to each imaging session. Hypocotyls were mounted in inhibitor solution and imaged immediately. CK-666 (Sigma-Aldrich; Cat # 182515; St. Louis, MO, USA) and SMIFH2 (Sigma-Aldrich; Cat # 344092) were dissolved in DMSO to prepare a 5 mM stock solution. FM4-64 (Invitrogen; Cat # T3166; Carlsbad, CA, USA) was dissolved in DMSO and used at 20 mM.

Live Cell Imaging

For both snapshot and time-lapse image acquisitions, epidermal cells from the apical region of 5-d-old dark-grown hypocotyls were used unless otherwise stated. All images and movies were collected using variable-angle epifluorescence microscopy (VAEM) with an Olympus TIRF objective (60X, 1.45 numerical aperture) as described previously (Cai et al., 2014; Cao et al., 2016; Henty et al., 2011; Li et al., 2012; Staiger et al., 2009).

For actin architecture analysis, more than 200 images of hypocotyl epidermal cells were collected from at least 15 individual seedlings per genotype or drug treatment. For single actin

filament dynamics analysis, more than 50 filaments from at least 10 hypocotyls were measured per genotype or drug treatment. For nucleation frequency analysis, more than 380 events from 15 hypocotyls were observed per genotype or drug treatment. All experiments were conducted with at least 3 biological repeats and one representative example is shown in each figure.

Image Processing and Quantitative Analysis of Actin Cytoskeleton Architecture and Single Actin Filament Dynamics

Images and movies were acquired using SlideBook software (version 5.5; Intelligent Imaging Innovations) and processed with Image J (Adobe Systems). All images used for actin architecture analysis were collected with a fixed exposure time, laser power, and camera gain setting.

To quantify actin architecture, four parameters, *density*, *skewness*, *angle*, and *parallelness*, were employed in this study; density and skewness measure the percentage of occupancy of GFP signal in an image and the extent of actin filament bundling respectively, angle and parallelness describe how filaments orient relative to the longitudinal axel of the cell or each other respectively (Arieti and Staiger, 2020; Cai et al., 2014; Cao et al., 2016; Henty et al., 2011; Higaki et al., 2010; Li et al., 2012; Ueda et al., 2010). Micrographs were analyzed in Image J using the methods described previously (Higaki et al., 2010; Henty et al., 2011; Li et al., 2012).

To compare single actin filament parameters between genotype or drug treatment, double-blind experiments (data collection and analysis) were performed. Maximum filament length and lifetime, filament severing frequency, elongation rates, filament convolutedness and the rage of change of convolutedness were measured as described previously (Cai et al., 2014; Cao et al., 2016; Henty et al., 2011; Li et al., 2012; Staiger et al., 2009). For nucleation frequency analysis, a 400 μm^2 ROI was randomly selected from movies of epidermal cells at the apical region of the hypocotyl, and all observable nucleation events were counted during a time period of 100 s, according to Cao et al., 2016. To account for differences in filament density in genotypes or drug treatments, the nucleation frequency was normalized against filament numbers in the ROI.

Statistical Analysis

One-way ANOVA with Tukey's post-hoc tests were performed in SPSS (version 25) to determine significance among different treatments. Two-tailed Student's t test was performed in Excel 15.32. Any difference with a P value over 0.05 was considered significantly different.

Supplemental Online Materials

Table S1. Single actin filament dynamics in wild type (*ARPC*2) and *arpc2* with or without CK-666.
Table S2. Actin filament shape change in control- and inhibitor-treated wild-type (Col-0) epidermal cells.
Figure S1. Actin filament nucleation frequency is decreased in *arpc2* and after treatment of wild type with CK-666.
Figure S2. CK-666 is an acute and reversible chemical inhibitor of the Arp2/3 complex in plant cells.
Figure S3. Actin architecture is perturbed in *arpc2* and the reduced filament density and bundling phenotypes are recapitulated by treatment with CK-666.
Figure S4. Actin filament density significantly increases after treatment of *arpc2* with the formin inhibitor SMIFH2.
Figure S5. Overall filament nucleation and *de novo* filament formation increase when ARPC2 and formin activity are simultaneously inhibited.
Figure S6. Filament convolutedness decreases when formin or myosin activities are inhibited.

Video 1. Full time-lapse sequence of actin filament nucleation activities in mock-treated wild-type (*ARP2*) cells.
Video 2. Full time-lapse sequence of actin filament nucleation activities in mock-treated *arp2-1* cells.
Video 3. Representative actin filament nucleated *de novo* from the cytoplasm (as in Fig. 3 A, top row).
Video 4. Representative actin filament nucleated from the side of a pre-existing filament (as in Fig. 3 A, middle row).
Video 5. Representative actin filament nucleated from the end of a pre-existing filament (as in Fig. 3 A, bottom row).
Video 6. Representative example of filament elongation (as in Fig. 4 A).
Video 7. Representative example of filament severing (as in Fig. 4 A).
Video 8. Full time-lapse sequence of actin filament nucleation activities in CK-666-treated wild-type (*ARP2*) cells.
Video 9. Full time-lapse sequence of actin filament nucleation activities in CK-666-treated *arp2-1* cells.
Video 10. Full time-lapse sequence of actin filament nucleation activities in SMIFH2-treated wild-type (*ARP2*) cells.
Video 11. Full time-lapse sequence of actin filament nucleation activities in SMIFH2-treated *arp2-1* cells.

Acknowledgments

We thank Hongbing Luo (Purdue University) for excellent care and maintenance of plant materials, Dan Szymanski (Purdue University) for providing the *arpc2* line, and David Kovar (University of Chicago) and Laurent Blanchoin (Interdisciplinary Research Institute of Grenoble) for helpful comments. We are also grateful to the Arabidopsis Biological Resource Center (Ohio State University) for supplying the *arp2-1* T-DNA insertion line. The TIRF microscopy facility was supported, in part, by the Bindley Bioscience Center at Purdue. This work was funded by a grant from the Physical Biosciences program of the US Department of Energy, Office of Basic Energy Sciences (DE-FG02-09ER15526) to C.J.S. Conceptualization of experiments and manuscript preparation by C.J.S. were supported by the EMBRIO Institute, an NSF-Biological Integration Institute under contract no. 2120200.

The authors declare no competing financial interests.

Author Contributions

L. Xu acquired and analyzed data, prepared figures, wrote and revised the manuscript; L. Cao acquired and analyzed data; J. Li acquired and analyzed data; C.J. Staiger conceptualized experiments, acquired funding, wrote and revised the manuscript.

References

Akin, O., and R.D. Mullins. 2008. Capping protein increases the rate of actin-based motility by promoting filament nucleation by the Arp2/3 complex. *Cell*. 133:841-851.

Ali, M.F., U. Fatema, X. Peng, S.W. Hacker, D. Maruyama, M.-X. Sun, and T. Kawashima. 2020. ARP2/3-independent WAVE/SCAR pathway and class XI myosin control sperm nuclear migration in flowering plants. *Proc. Natl. Acad. Sci. USA*. 117:32757-32763.

Amann, K.J., and T.D. Pollard. 2001. Direct real-time observation of actin filament branching mediated by Arp2/3 complex using total internal reflection fluorescence microscopy. *Proc. Natl. Acad. Sci. USA*. 98:15009-15013.

Antkowiak, A., A. Guillotin, M. Boiero Sanders, J. Colombo, R. Vincentelli, and A. Michelot. 2019. Sizes of actin networks sharing a common environment are determined by the relative rates of assembly. *PLoS Biol.* 17:e3000317.

Arieti, R.S., and C.J. Staiger. 2020. Auxin-induced actin cytoskeleton rearrangements require AUX1. *New Phytol.* 226:441-459.

Beltzner, C.C., and T.D. Pollard. 2008. Pathway of actin filament branch formation by Arp2/3 complex. *J. Biol. Chem.* 283:7135-7144.

Blanchoin, L., and A. Michelot. 2012. Actin cytoskeleton: a team effort during actin assembly. *Curr. Biol.* 22:R643-R645.

Blanchoin, L., and C.J. Staiger. 2010. Plant formins: Diverse isoforms and unique molecular mechanism. *Biochim. Biophys. Acta*. 1803:201-206.

Burke, T.A., J.R. Christensen, E. Barone, C. Suarez, V. Sirotkin, and D.R. Kovar. 2014. Homeostatic actin cytoskeleton networks are regulated by assembly factor competition for monomers. *Curr. Biol.* 24:579-585.

Burlacu, S., and J. Borejdo. 1992. Motion of actin filaments in the presence of myosin heads and ATP. *Biophys. J.* 63:1471-1482.

Cabrera, R., J. Suo, E. Young, and E.C. Chang. 2011. *Schizosaccharomyces pombe* Arc3 is a conserved subunit of the Arp2/3 complex required for polarity, actin organization, and endocytosis. *Yeast*. 28:495-503.

Cai, C., J.L. Henty-Ridilla, D.B. Szymanski, and C.J. Staiger. 2014. Arabidopsis myosin XI: a motor rules the tracks. *Plant Physiol.* 166:1359-1370.

Cao, L., J.L. Henty-Ridilla, L. Blanchoin, and C.J. Staiger. 2016. Profilin-dependent nucleation and assembly of actin filaments controls cell elongation in Arabidopsis. *Plant Physiol.* 170:220-233.

Chan, F.Y., A.M. Silva, J. Saramago, J. Pereira-Sousa, H.E. Brighton, M. Pereira, K. Oegema, R. Gassmann, and A.X. Carvalho. 2019. The ARP2/3 complex prevents excessive formin activity during cytokinesis. *Mol. Biol. Cell*. 30:96-107.

Cheung, A.Y., and H.-m. Wu. 2004. Overexpression of an Arabidopsis formin stimulates supernumerary actin cable formation from pollen tube cell membrane. *Plant Cell*. 16:257-269.

Cifrová, P., D. Oulehlová, E. Kollárová, J. Martinek, A. Rosero, V. Žárský, K. Schwarzerová, and F. Cvrčková. 2020. Division of labor between two actin nucleators-the formin FH1 and the ARP2/3 complex-in *Arabidopsis* epidermal cell morphogenesis. *Front. Plant Sci.* 11:148.

Cvrčková, F. 2013. Formins and membranes: anchoring cortical actin to the cell wall and beyond. *Front. Plant Sci.* 4:436.

Cvrčková, F., B. Bavlnka, and V. Žárský. 2000. Identification and cloning of AtFORMIN1, an *Arabidopsis thaliana* formin homologue. *Biochem. Soc. Trans.* 28:A208-A208.

Cvrčková, F., M. Novotný, D. Pícková, and V. Žárský. 2004. Formin homology 2 domains occur in multiple contexts in angiosperms. *BMC Genomics*. 5:44.

Davidson, A.J., C. Amato, P.A. Thomason, and R.H. Insall. 2018. WASP family proteins and formins compete in pseudopod- and bleb-based migration. *J. Cell Biol.* 217:701-714.
Dayel, M.J., E.A. Holleran, and R.D. Mullins. 2001. Arp2/3 complex requires hydrolyzable ATP for nucleation of new actin filaments. *Proc. Natl. Acad. Sci. USA*. 98:14871-14876.
Dayel, M.J., and R.D. Mullins. 2004. Activation of Arp2/3 complex: addition of the first subunit of the new filament by a WASP protein triggers rapid ATP hydrolysis on Arp2. *PLoS Biol.* 2:476-485.
Deeks, M.J., P.J. Hussey, and B. Davies. 2002. Formins: intermediates in signal-transduction cascades that affect cytoskeletal reorganization. *Trends Plant Sci.* 7:492-498.
Di Nardo, A., G. Cicchetti, H. Falet, J.H. Hartwig, T.P. Stossel, and D.J. Kwiatkowski. 2005. Arp2/3 complex-deficient mouse fibroblasts are viable and have normal leading-edge actin structure and function. *Proc. Natl. Acad. Sci. USA*. 102:16263-16268.
El-Assal, S.E.-D., J. Le, D. Basu, E.L. Mallery, and D.B. Szymanski. 2004. DISTORTED2 encodes an ARPC2 subunit of the putative *Arabidopsis* ARP2/3 complex. *Plant J.* 38:526-538.
Facette, M.R., Y. Park, D. Sutimantanapi, A. Luo, H.N. Cartwright, B. Yang, E.J. Bennett, A.W. Sylvester, and L.G. Smith. 2015. The SCAR/WAVE complex polarizes PAN receptors and promotes division asymmetry in maize. *Nat. Plants*. 1:14024.
Fujiwara, I., S. Suetsugu, S. Uemura, T. Takenawa, and S. Ishiwata. 2002. Visualization and force measurement of branching by Arp2/3 complex and N-WASP in actin filament. *Biochem. Biophys. Res. Commun.* 293:1550-1555.
Funk, J., F. Merino, L. Venkova, L. Heydenreich, J. Kierfeld, P. Vargas, S. Raunser, M. Piel, and P. Bieling. 2019. Profilin and formin constitute a pacemaker system for robust actin filament growth. *eLife*. 8.
García-González, J., S.t.p.n. Kebrlová, M. Semerák, J. Lacek, I. Kotannal Baby, J. Petrášek, and K. Schwarzerová. 2020. Arp2/3 complex is required for auxin-driven cell expansion through regulation of auxin transporter homeostasis. *Front. Plant Sci.* 11:486.
Goley, E.D., and M.D. Welch. 2006. The ARP2/3 complex: an actin nucleator comes of age. *Nat. Rev. Mol. Cell Biol.* 7:713-726.
Hardham, A.R., D.A. Jones, and D. Takemoto. 2007. Cytoskeleton and cell wall function in penetration resistance. *Curr. Opin. Plant Biol.* 10:342-348.
Harries, P.A., A. Pan, and R.S. Quatrano. 2005. Actin-related protein2/3 complex component ARPC1 is required for proper cell morphogenesis and polarized cell growth in *Physcomitrella patens*. *Plant Cell*. 17:2327-2339.
Henty, J.L., S.W. Bledsoe, P. Khurana, R.B. Meagher, B. Day, L. Blanchoin, and C.J. Staiger. 2011. *Arabidopsis* actin depolymerizing factor4 modulates the stochastic dynamic behavior of actin filaments in the cortical array of epidermal cells. *Plant Cell*. 23:3711-3726.
Henty-Ridilla, J.L., J. Li, L. Blanchoin, and C.J. Staiger. 2013a. Actin dynamics in the cortical array of plant cells. *Curr. Opin. Plant Biol.* 16:678-687.
Henty-Ridilla, J.L., M. Shimono, J. Li, J.H. Chang, B. Day, and C.J. Staiger. 2013b. The plant actin cytoskeleton responds to signals from microbe-associated molecular patterns. *PLoS Pathog.* 9:e1003290.
Hetrick, B., M.S. Han, L.A. Helgeson, and B.J. Nolen. 2013. Small molecules CK-666 and CK-869 inhibit actin-related protein 2/3 complex by blocking an activating conformational change. *Chem. Biol.* 20:701-712.
Higaki, T., N. Kutsuna, T. Sano, N. Kondo, and S. Hasezawa. 2010. Quantification and cluster analysis of actin cytoskeletal structures in plant cells: role of actin bundling in stomatal movement during diurnal cycles in Arabidopsis guard cells. *Plant J.* 61:156-165.
Hotulainen, P., and P. Lappalainen. 2006. Stress fibers are generated by two distinct actin assembly mechanisms in motile cells. *J. Cell Biol*. 173:383-394.

Ichetovkin, I., W. Grant, and J. Condeelis. 2002. Cofilin produces newly polymerized actin filaments that are preferred for dendritic nucleation by the Arp2/3 complex. *Curr. Biol.* 12:79-84.

Jasnin, M., F. Beck, M. Ecke, Y. Fukuda, A. Martinez-Sanchez, W. Baumeister, and G. Gerisch. 2019. The architecture of traveling actin waves revealed by cryo-electron tomography. *Structure*. 27:1211-1223 e1215.

Jiang, K., K. Sorefan, M.J. Deeks, M.W. Bevan, P.J. Hussey, and A.M. Hetherington. 2012. The ARP2/3 complex mediates guard cell actin reorganization and stomatal movement in *Arabidopsis*. *Plant Cell*. 24:2031-2040.

Kadzik, R.S., K.E. Homa, and D.R. Kovar. 2020. F-actin cytoskeleton network self-organization through competition and cooperation. *Annu. Rev. Cell Dev. Biol.* 36:35-60.

Kahr, W.H.A., F.G. Pluthero, A. Elkadri, N. Warner, M. Drobac, C.H. Chen, R.W. Lo, L. Li, R. Li, Q. Li, C. Thoeni, J. Pan, G. Leung, I. Lara-Corrales, R. Murchie, E. Cutz, R.M. Laxer, J. Upton, C.M. Roifman, R.S.M. Yeung, J.H. Brumell, and A.M. Muise. 2017. Loss of the Arp2/3 complex component ARPC1B causes platelet abnormalities and predisposes to inflammatory disease. *Nat. Commun.* 8:14816.

Kovar, D.R. 2006. Molecular details of formin-mediated actin assembly. *Curr. Opin. Cell Biol.* 18:11-17.

Kovar, D.R., J.R. Kuhn, A.L. Tichy, and T.D. Pollard. 2003. The fission yeast cytokinesis formin Cdc12p is a barbed end actin filament capping protein gated by profilin. *J. Cell Biol.* 161:875-887.

Kovar, D.R., and T.D. Pollard. 2004. Progressing actin: Formin as a processive elongation machine. *Nat. Cell Biol.* 6:1158-1159.

Lan, Y., X. Liu, Y. Fu, and S. Huang. 2018. *Arabidopsis* class I formins control membrane-originated actin polymerization at pollen tube tips. *PLOS Genet.* 14:e1007789.

Le, J., S.E.-D. El-Assal, D. Basu, M.E. Saad, and D.B. Szymanski. 2003. Requirements for *Arabidopsis* ATARP2 and ATARP3 during epidermal development. *Curr. Biol.* 13:1341-1347.

Li, J., J.L. Henty-Ridilla, S. Huang, X. Wang, L. Blanchoin, and C.J. Staiger. 2012. Capping protein modulates the dynamic behavior of actin filaments in response to phosphatidic acid in *Arabidopsis*. *Plant Cell*. 24:3742-3754.

Li, S., L. Blanchoin, Z. Yang, and E.M. Lord. 2003. The putative Arabidopsis Arp2/3 complex controls leaf cell morphogenesis. *Plant Physiol.* 132:2034-2044.

Li, X., J.-H. Li, W. Wang, N.-Z. Chen, T.-S. Ma, Y.-N. Xi, X.-L. Zhang, H.-F. Lin, Y. Bai, S.-J. Huang, and Y.-L. Chen. 2014. ARP2/3 complex-mediated actin dynamics is required for hydrogen peroxide-induced stomatal closure in Arabidopsis. *Plant Cell Environ.* 37:1548-1560.

Liu, H.-K., Y.-J. Li, S.-J. Wang, T.-L. Yuan, W.-J. Huang, X. Dong, J.-Q. Pei, D. Zhang, S. McCormick, and W.-H. Tang. 2020. Kinase partner protein plays a key role in controlling the speed and shape of pollen tube growth in tomato. *Plant Physiol.* 184:1853-1869.

Lomakin, A.J., K.-C. Lee, S.J. Han, D.A. Bui, M. Davidson, A. Mogilner, and G. Danuser. 2015. Competition for actin between two distinct F-actin networks defines a bistable switch for cell polarization. *Nat. Cell Biol.* 17:1435-1445.

Mathur, J., N. Mathur, B. Kernebeck, and M. Hulskamp. 2003a. Mutations in actin-related proteins 2 and 3 affect cell shape development in Arabidopsis. *Plant Cell*. 15:1632-1645.

Mathur, J., N. Mathur, V. Kirik, B. Kernebeck, B.P. Srinivas, and M. Hulskamp. 2003b. *Arabidopsis* CROOKED encodes for the smallest subunit of the ARP2/3 complex and controls cell shape by region specific fine F-actin formation. *Development*. 130:3137-3146.

Michelot, A., E. Derivery, R. Paterski-Boujemaa, C. Guerin, S. Huang, F. Parcy, C.J. Staiger, and L. Blanchoin. 2006. A novel mechanism for the formation of actin-filament bundles by a nonprocessive formin. *Curr. Biol.* 16:1924-1930.

Michelot, A., A. Grassart, V. Okreglak, M. Costanzo, C. Boone, and D.G. Drubin. 2013. Actin Filament Elongation in Arp2/3-Derived Networks Is Controlled by Three Distinct Mechanisms. *Dev. Cell*. 24:182-195.

Michelot, A., C. Guérin, S. Huang, M. Ingouff, S.p. Richard, N. Rodiuc, C.J. Staiger, and L. Blanchoin. 2005. The formin homology 1 domain modulates the actin nucleation and bundling activity of Arabidopsis FORMIN1. *Plant Cell*. 17:2296-2313.

Miller, K.G., C.M. Field, and B.M. Alberts. 1989. Actin-binding proteins from Drosophila embryos: a complex network of interacting proteins detected by F-actin affinity chromatography. *J. Cell Biol*. 109:2963-2975.

Mullins, R.D., J.A. Heuser, and T.D. Pollard. 1998. The interaction of Arp2/3 complex with actin: Nucleation, high affinity pointed end capping, and formation of branching networks of filaments. *Proc. Natl. Acad. Sci. USA*. 95:6181-6186.

Nishimura, Y., S. Shi, Q. Li, A.D. Bershadsky, and V. Viasnoff. 2021. Crosstalk between myosin II and formin functions in the regulation of force generation and actomyosin dynamics in stress fibers. *Cells Dev.* 168:203736.

Nolen, B.J., N. Tomasevic, A. Russell, D.W. Pierce, Z. Jia, C.D. McCormick, J. Hartman, R. Sakowicz, and T.D. Pollard. 2009. Characterization of two classes of small molecule inhibitors of Arp2/3 complex. *Nature*. 460:1031-1034.

Orman, M., M. Landis, A. Oza, D. Nambiar, J. Gjeci, K. Song, V. Huang, A. Klestzick, C. Hachicho, S.Q. Liu, J.M. Kamm, F. Bartolini, J.J. Vadakkan, C.M. Rojas, and C.L. Vizcarra. 2022. Alterations to the broad-spectrum formin inhibitor SMIFH2 improve potency. *bioRxiv.* doi: 10.1101/2022.03.10.483826

Paul, A.S., and T.D. Pollard. 2008. The role of the FH1 domain and profilin in formin-mediated actin-filament elongation and nucleation. *Curr. Biol.* 18:9-19.

Peng, X., T. Yan, and M. Sun. 2017. The WASP-Arp2/3 complex signal cascade is involved in actin-dependent sperm nuclei migration during double fertilization in tobacco and maize. *Sci. Rep.* 7:43161.

Pollard, T.D. 2007. Regulation of actin filament assembly by Arp2/3 complex and formins. *Annu. Rev. Biophys. Biomol. Struct.* 36:451-477.

Pollard, T.D., L. Blanchoin, and R.D. Mullins. 2000. Molecular mechanisms controlling actin filament dynamics in nonmuscle cells. *Annu. Rev. Biophys. Biomol. Struct.* 29:545-576.

Qin, L., L. Liu, J. Tu, G. Yang, S. Wang, T.D. Quilichini, P. Gao, H. Wang, G. Peng, E.B. Blancaflor, R. Datla, D. Xiang, K.E. Wilson, and Y. Wei. 2021. The ARP2/3 complex, acting cooperatively with Class I formins, modulates penetration resistance in Arabidopsis against powdery mildew invasion. *Plant Cell*. 33:3151-3175.

Roh-Johnson, M., and B. Goldstein. 2009. In vivo roles for Arp2/3 in cortical actin organization during *C. elegans* gastrulation. *J. Cell Sci.* 122:3983-3993.

Romero, S., C. Le Clainche, D. Didry, C. Egile, D. Pantaloni, and M.-F. Carlier. 2004. Formin is a processive motor that requires profilin to accelerate actin assembly and associated ATP hydrolysis. *Cell*. 119:419-429.

Rosenbloom, A.D., E.W. Kovar, D.R. Kovar, L.M. Loew, and T.D. Pollard. 2021. Mechanism of actin filament nucleation. *Biophys. J.* 120:4399-4417.

Rosero, A., V. Žárský, and F. Cvrčková. 2013. AtFH1 formin mutation affects actin filament and microtubule dynamics in *Arabidopsis thaliana*. *J. Exp. Bot.* 64:585-597.

Rouiller, I., X.-P. Xu, K.J. Amann, C. Egile, S. Nickell, D. Nicastro, R. Li, T.D. Pollard, N. Volkmann, and D. Hanein. 2008. The structural basis of actin filament branching by the Arp2/3 complex. *J. Cell Biol*. 180:887-895.

Sahi, V.P., P. Cifrová, J. García-González, I. Kotannal Baby, G. Mouillé, E. Gineau, K. Müller, F. Baluška, A. Soukup, J. Petrášek, and K.I. Schwarzerová. 2018. *Arabidopsis thaliana* plants lacking the ARP2/3 complex show defects in cell wall assembly and auxin distribution. *Ann. Bot.* 122:777-789.

Sartori-Rupp, A., D. Cordero Cervantes, A. Pepe, K. Gousset, E. Delage, S. Corroyer-Dulmont, C. Schmitt, J. Krijnse-Locker, and C. Zurzolo. 2019. Correlative cryo-electron microscopy reveals the structure of TNTs in neuronal cells. *Nat. Commun.* 10:342.

Sept, D., and J.A. McCammon. 2001. Thermodynamics and kinetics of actin filament nucleation. *Biophys. J.* 81:667-674.

Sheahan, M.B., C.J. Staiger, R.J. Rose, and D.W. McCurdy. 2004. A green fluorescent protein fusion to actin-binding domain 2 of Arabidopsis fimbrin highlights new features of a dynamic actin cytoskeleton in live plant cells. *Plant Physiol.* 136:3968-3978.

Staiger, C.J., N.S. Poulter, J.L. Henty, V.E. Franklin-Tong, and L. Blanchoin. 2010. Regulation of actin dynamics by actin-binding proteins in pollen. *J. Exp. Bot.* 61:1969-1986.

Staiger, C.J., M.B. Sheahan, P. Khurana, X. Wang, D.W. McCurdy, and L. Blanchoin. 2009. Actin filament dynamics are dominated by rapid growth and severing activity in the *Arabidopsis* cortical array. *the Journal of Cell Biology*. 184:269-280.

Stürner, T., A. Tatarnikova, J. Mueller, B. Schaffran, H. Cuntz, Y. Zhang, M. Nemethova, S. Bogdan, V. Small, and G. Tavosanis. 2019. Transient localization of the Arp2/3 complex initiates neuronal dendrite branching in vivo. *Development*. 146.

Suarez, C., R.T. Carroll, T.A. Burke, J.R. Christensen, A.J. Bestul, J.A. Sees, M.L. James, V. Sirotkin, and D.R. Kovar. 2015. Profilin regulates F-actin network homeostasis by favoring formin over Arp2/3 complex. *Dev. Cell*. 32:43-53.

Sun, S.-C., Q.-L. Wang, W.-W. Gao, Y.-N. Xu, H.-L. Liu, X.-S. Cui, and N.-H. Kim. 2013. Actin nucleator Arp2/3 complex is essential for mouse preimplantation embryo development. *Reprod. Fertil. Dev.* 25:617-623.

Szymanski, D.B., M.D. Marks, and S.M. Wick. 1999. Organized F-actin is essential for normal trichome morphogenesis in Arabidopsis. *Plant Cell*. 11:2331-2347.

Ueda, H., E. Yokota, N. Kutsuna, T. Shimada, K. Tamura, T. Shimmen, S. Hasezawa, V.V. Dolja, and I. Hara-Nishimura. 2010. Myosin-dependent endoplasmic reticulum motility and F-actin organization in plant cells. *Proc. Natl. Acad. Sci. USA*. 107:6894-6899.

van der Kammen, R., J.-Y. Song, I. de Rink, H. Janssen, S. Madonna, C. Scarponi, C. Albanesi, W. Brugman, and M. Innocenti. 2017. Knockout of the Arp2/3 complex in epidermis causes a psoriasis-like disease hallmarked by hyperactivation of transcription factor Nrf2. *Development*. 144:4588-4603.

Vaškovičová, K., V. Žárský, D. Rösel, M. Nikolič, R. Buccione, F. Cvrčková, and J. Brábek. 2013. Invasive cells in animals and plants: searching for LECA machineries in later eukaryotic life. *Biol. Direct*. 8:8.

Vavylonis, D., D.R. Kovar, B. O'Shaughnessy, and T.D. Pollard. 2006. Model of formin-associated actin filament elongation. *Mol. Cell*. 21:455-466.

Vidali, L., P.A.C. van Gisbergen, C. Guerin, P. Franco, M. Li, G.M. Burkart, R.C. Augustine, L. Blanchoin, and M. Bezanilla. 2009. Rapid formin-mediated actin-filament elongation is essential for polarized plant cell growth. *Proc. Natl. Acad. Sci. USA*. 106:13341-13346.

Wang, P., R. Pleskot, J. Zang, J. Winkler, J. Wang, K. Yperman, T. Zhang, K. Wang, J. Gong, Y. Guan, C. Richardson, P. Duckney, M. Vandorpe, E. Mylle, J. Fiserova, D. Van Damme, and P.J. Hussey. 2019. Plant AtEH/Pan1 proteins drive autophagosome formation at ER-PM contact sites with actin and endocytic machinery. *Nat. Commun.* 10:5132.

Wang, P., C. Richardson, C. Hawes, and P.J. Hussey. 2016. *Arabidopsis* NAP1 Regulates the Formation of Autophagosomes. *Curr. Biol.* 26:2060-2069.

Winter, D.C., E.Y. Choe, and R. Li. 1999. Genetic dissection of the budding yeast Arp2/3 complex: a comparison of the *in vivo* and structural roles of individual subunits. *Proc. Natl. Acad. Sci. USA*. 96:7288-7293.

Yanagisawa, M., J.M. Alonso, and D.B. Szymanski. 2018. Microtubule-dependent confinement of a cell signaling and actin polymerization control module regulates polarized cell growth. *Curr. Biol.* 28:2459-2466.e2454.

Yanagisawa, M., A.S. Desyatova, S.A. Belteton, E.L. Mallery, J.A. Turner, and D.B. Szymanski. 2015. Patterning mechanisms of cytoskeletal and cell wall systems during leaf trichome morphogenesis. *Nat. Plants*. 1:15014.

Yanagisawa, M., C. Zhang, and D.B. Szymanski. 2013. ARP2/3-dependent growth in the plant kingdom: SCARs for life. *Front. Plant Sci.* 4:166.

Zhang, S., C. Liu, J. Wang, Z. Ren, C.J. Staiger, and H. Ren. 2016. A processive *Arabidopsis* formin modulates actin filament dynamics in association with profilin. *Mol. Plant*. 9:900-910.

Zhang, W., C. Cai, and C.J. Staiger. 2019. Myosins XI are involved in exocytosis of cellulose synthase complexes. *Plant Physiol.* 179:1537-1555.

Zhang, W., L. Huang, C. Zhang, and C.J. Staiger. 2021. Arabidopsis myosin XIK interacts with the exocyst complex to facilitate vesicle tethering during exocytosis. *Plant Cell*. 33:2454-2478.

Figures & Figure Legends

Table 1. Single actin filament dynamics in wild type (*ARP2*) and *arp2-1* mutant with or without CK-666.

Stochastic Dynamic Parameters	Genotype & Treatment			
	***ARP2* w/ mock**	***arp2-1* w/ mock**	***ARP2* w/ CK-666**	***arp2-1* w/ CK-666**
Elongation Rate; µm/s	1.75 ± 0.10 [a]	1.89 ± 0.10 [b]	1.91 ± 0.11 [b]	1.87 ± 0.10 [b]
Max. Filament length; µm	16.5 ± 0.5 [a]	17.1 ± 0.5 [b]	17.0 ± 0.5 [b]	17.3 ± 0.5 [b]
Max. Filament Lifetime; s	21.8 ± 1.0 [a]	23.1 ± 1.0 [b]	23.0 ± 1.0 [b]	22.9 ± 1.0 [b]
Severing Frequency; breaks/µm/s	0.008 ± 0.001 [a]	0.008 ± 0.001 [a]	0.008 ± 0.001 [a]	0.008 ± 0.001 [a]

Measurements were taken from the elongation apical region of 5-day-old dark-grown hypocotyls.
Values represent mean ± SE. n ≥ 50 filaments from at least 10 hypocotyls per treatment. One-way ANOVA with Tukey's post-hoc test, letters [a-b] denote genotypes/treatments that show statistically significant differences with other genotypes/treatments, $P < 0.05$

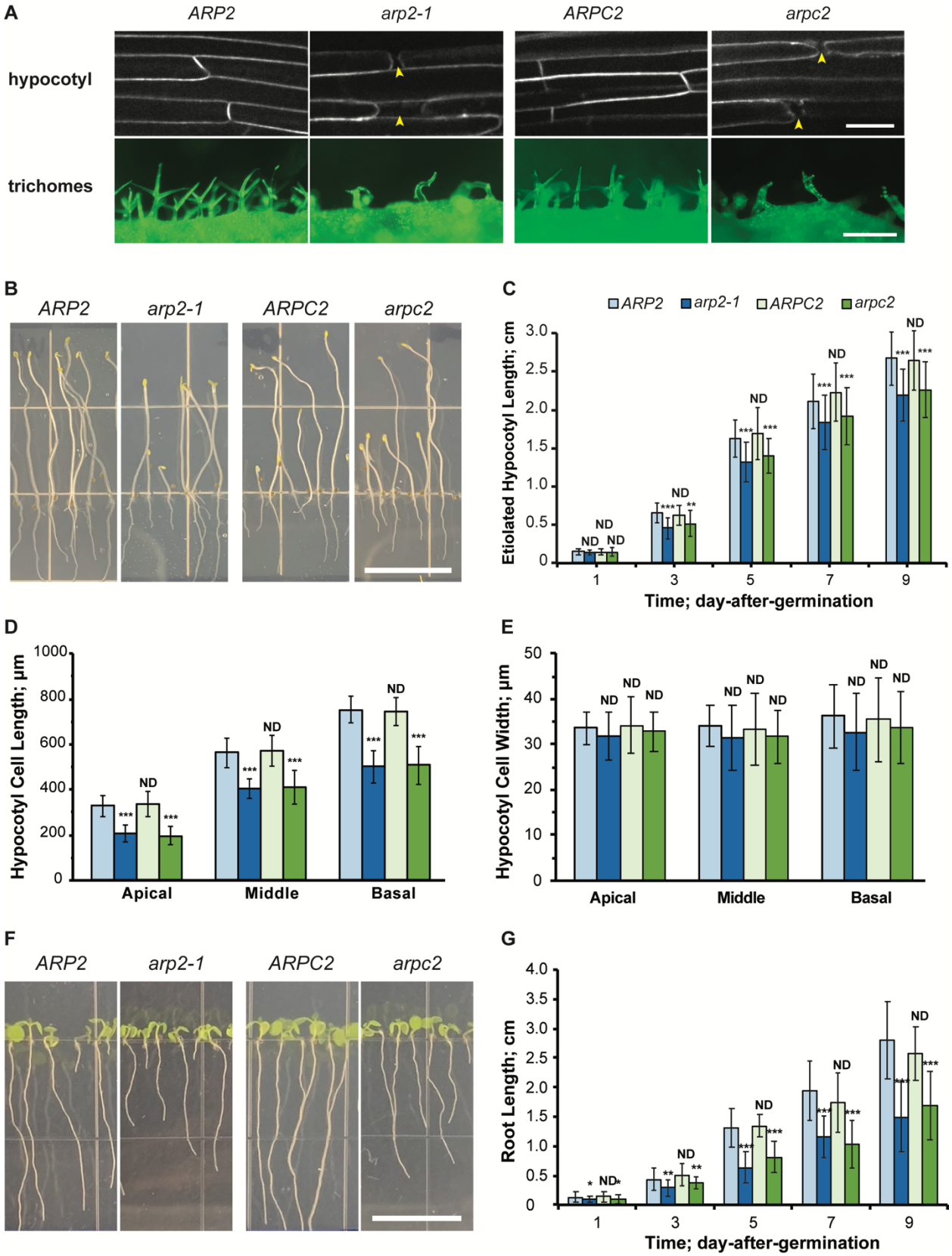
A
ARP2
arp2-1
ARPC2
arpc2
hypocotyl
trichomes
B
ARP2
arp2-1
ARPC2
arpc2
C
ARP2
arp2-1
ARPC2
arpc2
Etiolated Hypocotyl Length; cm
Time; day-after-germination
D
Hypocotyl Cell Length; µm
Apical
Middle
Basal
E
Hypocotyl Cell Width; µm
Apical
Middle
Basal
F
ARP2
arp2-1
ARPC2
arpc2
G
Root Length; cm
Time; day-after-germination

Figure 1. Disruption of the Arp2/3 complex leads to abnormal epidermal cell morphology and inhibits normal plant growth.

(A) Representative images of epidermal cells from 5-day-old etiolated hypocotyls of homozygous *arp2/3* complex mutants, *arp2-1* and *arpc2*, and their corresponding wild-type siblings (*ARP2* and *ARPC2*). Cells in *arp2-1* and *arpc2* had visible cell adhesion defects (yellow arrowheads) at end walls compared to wild-type siblings. Bar = 10 µm. Representative images of trichomes from young leaves of 2-week-old plants. Trichomes on *arp2-1* and *arpc2* leaves were severely distorted compared to wild-type siblings. Bar = 8 µm. **(B)** Representative images of 5-day-old dark grown seedlings. Bar = 1.0 cm. **(C)** Hypocotyls from *arp2-1* and *arpc2* were significantly shorter than their wild-type siblings over a developmental timeseries. **(D)** and **(E)** Quantitative analysis of average length **(D)** and width **(E)** of epidermal cells from the apical, middle, and basal regions of 5-day-old etiolated hypocotyls. **(F)** Representative images of 5-day-old light grown seedlings of *ARP2*, *arp2-1*, *ARPC2* and *arpc2*. Bar = 1.0 cm. **(G)** Roots from *arp2-1* and *arpc2* were significantly shorter than their wild-type siblings over a developmental timeseries. Values in **(C)** and **(G)** represent mean ± SE. $n \geq 50$ seedlings per genotype (Student's t test, ** $P < 0.005$, *** $P < 0.001$). Values in **(D)** and **(E)** represent mean ± SE. $n \geq 300$ cells from at least 10 hypocotyls per genotype (Student's t test, ** $P < 0.005$, *** $P < 0.001$).

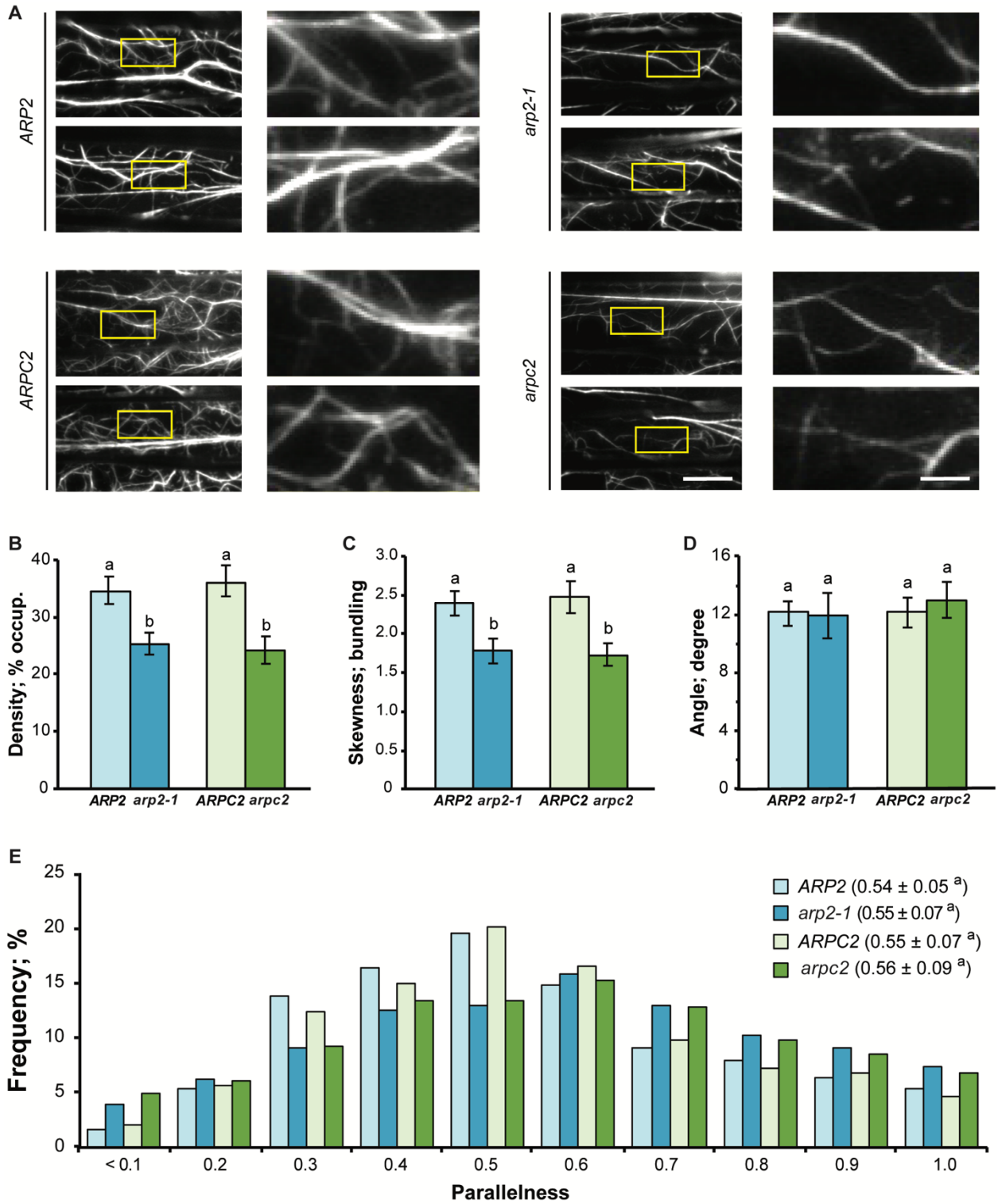

Figure 2. Genetic disruption of the Arp2/3 complex leads to reduced filament density and bundling.

(A) Representative images of epidermal cells from the apical region of 5-day-old etiolated hypocotyls expressing GFP-fABD2 imaged by variable angle epifluorescence microscopy (VAEM) are shown in the left columns. Bar = 20 µm. Regions of interest (yellow box) from figures at left were magnified and

shown in the right columns. Bar = 5 um. **(B)** and **(C)**, Quantitative analysis of the percentage of occupancy or density of actin filament arrays **(B)** and the extent of filament bundling or skewness **(C)**. Both the density and the bundling of actin arrays in *arp2-1* and *arpc2* cells were significantly decreased compared to those in wild-type cells. **(D)** Quantitative analysis of the average angle of actin filaments relative to the longitudinal axis of hypocotyl epidermal cells. There was no significant difference in the average angle of actin arrays between wild-type and mutant cells. **(E)** Quantitative analysis of the population distribution and average parallelness of actin filaments. There was no significant difference in the average parallelness of actin arrays between wild-type and mutant cells; however, the population distributions of *arp2-1* and *arpc2* were more left skewed compared to the respective wild type. Values in **(B)** to **(D)** represent mean ± SE. $n \geq 300$ cells from at least 15 hypocotyls per genotype (One-way ANOVA with Tukey's post-hoc test, letters [a-c] denote genotypes that show statistically significant differences with other treatments, $P < 0.05$).

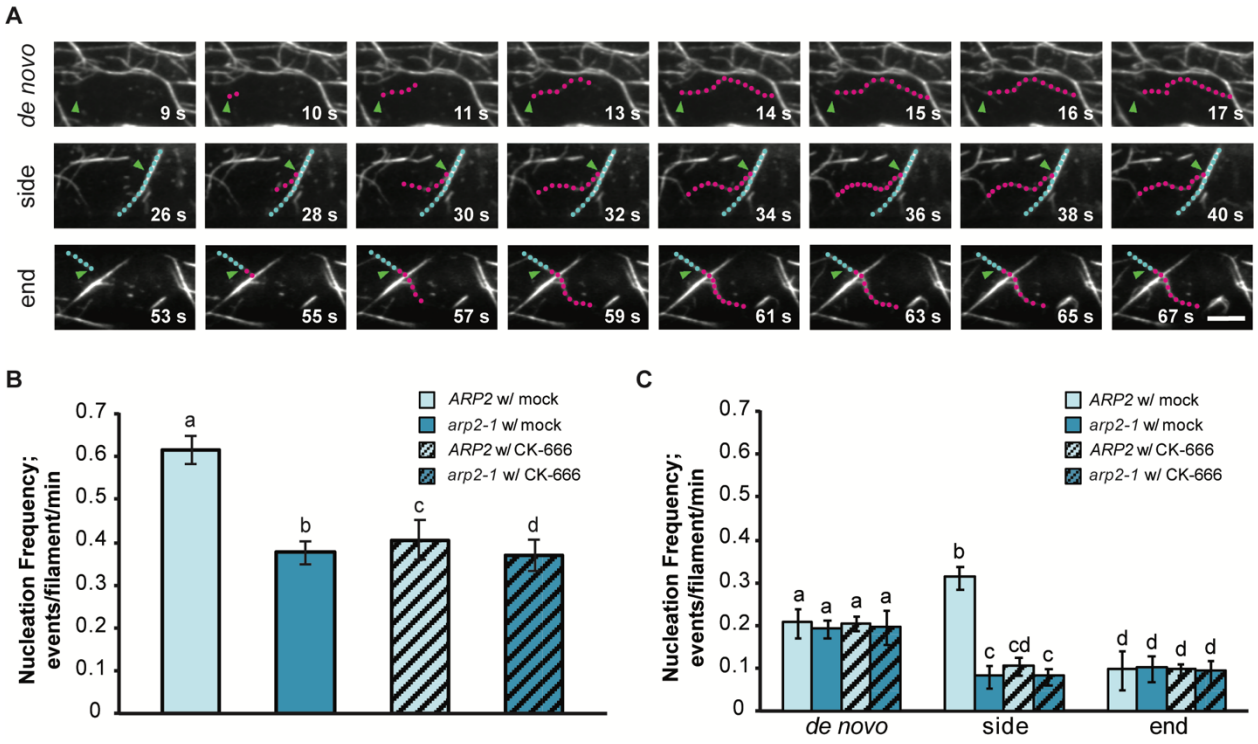

Figure 3. Actin filament nucleation frequency is decreased by chemical or genetic inhibition of the Arp2/3 complex.

(A) Representative time lapse series showing three subclasses of actin filament origin identified in hypocotyl epidermal cells: Actin filaments initiated *de novo* in the cytoplasm (top), from the side of a pre-existing filament (middle), or from the end of a pre-existing filament (bottom row). Blue dots; pre-existing filament. Magenta dots; new growing filament. Green arrowheads; nucleation sites. Bar = 5 µm. **(B)** and **(C)**, Quantitative analysis of actin filament nucleation frequency. The overall nucleation frequency for each genotype or treatment was defined as the total number of filament origins per filament per minute in a 400 μm^2 region of interest. Total nucleation frequency **(B)** in mock-treated wild-type cells (*ARP2*) was significantly higher than mock-treated *arp2-1*, CK-666-treated wild-type, or CK-666-treated *arp2-1* cells. When filament origin events were categorized into *de novo*, side, and end populations **(C)**, only the side-branching nucleation events showed a significant reduction in *arp2-1* and CK-666-treated cells compared to mock-treated wild type. Values in **(B)** and **(C)** represent mean ± SE. n ≥ 350 total events from at least 15 hypocotyls per treatment or genotype (One-way ANOVA with Tukey's post-hoc test, letters [a-d] denote treatments that show statistically significant differences with other treatments or genotypes, $P < 0.05$).

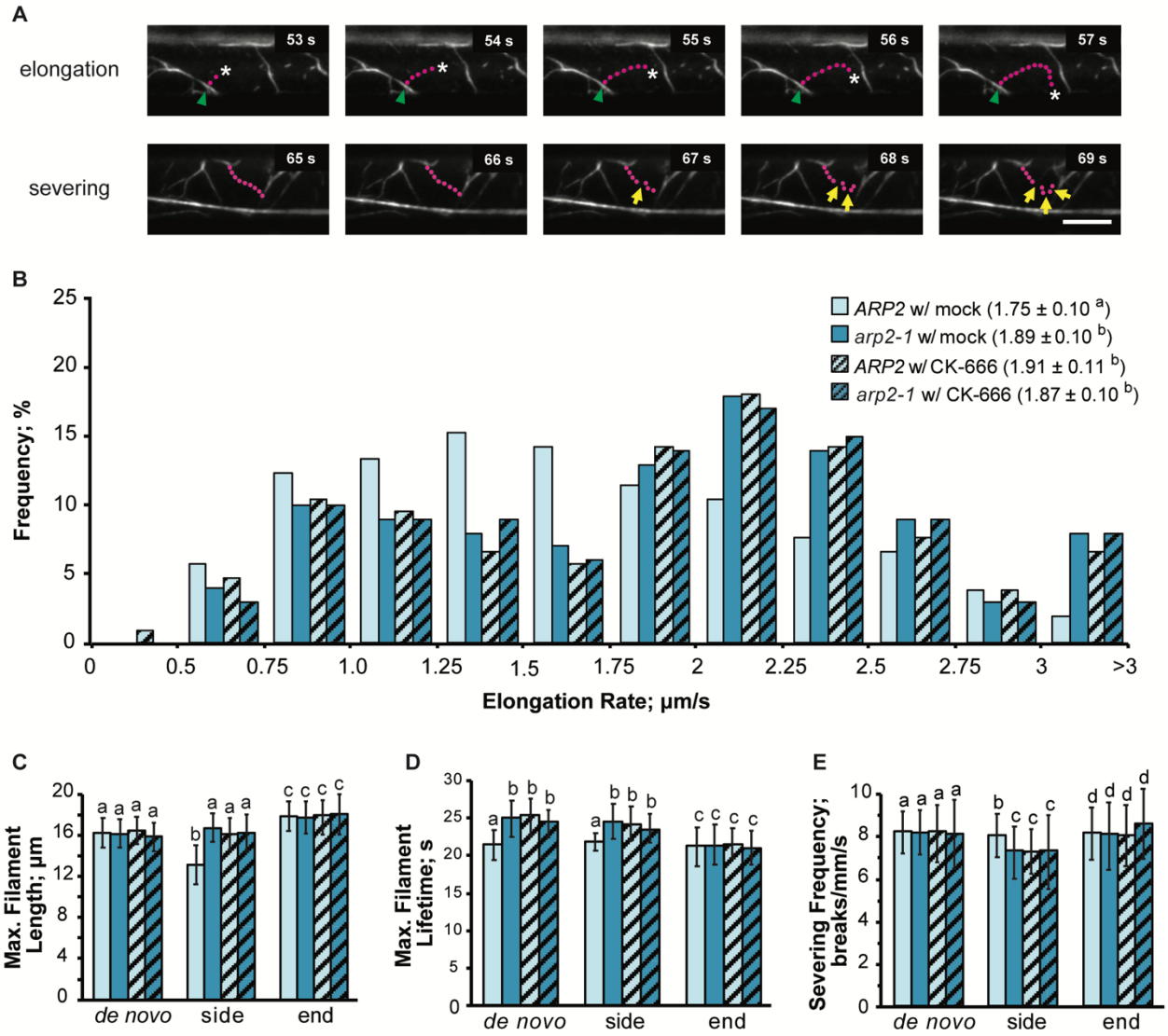

Figure 4. Actin filament dynamic properties are altered when the Arp2/3 complex is inhibited.

(A) A representative actin filament tracked during the elongation phase (top) and another filament is fragmented into pieces during the severing phase (bottom). Magenta dots; actin filament. Green arrowhead; nucleation site. White asterisk; elongating filament end. Yellow arrows; severing events. Bar = 10 µm. **(B)** Quantitative analysis of the population distribution and average elongation rate of actin filaments in hypocotyl epidermal cells. The average elongation rate of filaments from mock-treated wild-type cells was significantly lower than the ones from mock-treated *arp2-1*, CK-666-treated wild-type, and CK-666- treated *arp2-1* cells; the elongation rate distribution of mock-treated wild type had a single peak at 1.25 – 1.5 µm/s whereas the Arp2/3-inhibited groups had three peaks at 0.75 – 1.25 µm/s, 2.0 – 2.25 µm/s, and > 3 µm/s. **(C)** Average maximum length of side-branching filaments in mock-treated wild type cells was significantly longer than those in mock-treated *arp2-1*, CK-666-treated wild-type, or CK-666-treated *arp2-1* cells; however, filaments that originated *de novo* or from pre-existing ends did not show any significant difference. **(D)** Average maximum lifetime of side-branching filaments in mock-treated wild-type cells was significantly shorter than the ones from mock-treated *arp2-1*, CK-666-treated wild-type, or CK-666-treated *arp2-1* cells; however, filaments that originated *de novo* or from pre-existing ends did not show any significant difference. **(E)** Severing frequencies of side-branching filaments in

mock-treated *arp2-1*, CK-666-treated wild-type, or CK-666-treated *arp2-1* cells were significantly lower than filaments from other origins in both wild-type and *arp2-1* cells despite the treatment type. Values in **(B)** to **(E)** represent mean ± SE. n ≥ 50 single filaments from at least 10 hypocotyls per treatment (One-way ANOVA with Tukey's post-hoc test, letters [a-d] denote treatments that show statistically significant differences with other treatments, $P < 0.05$).

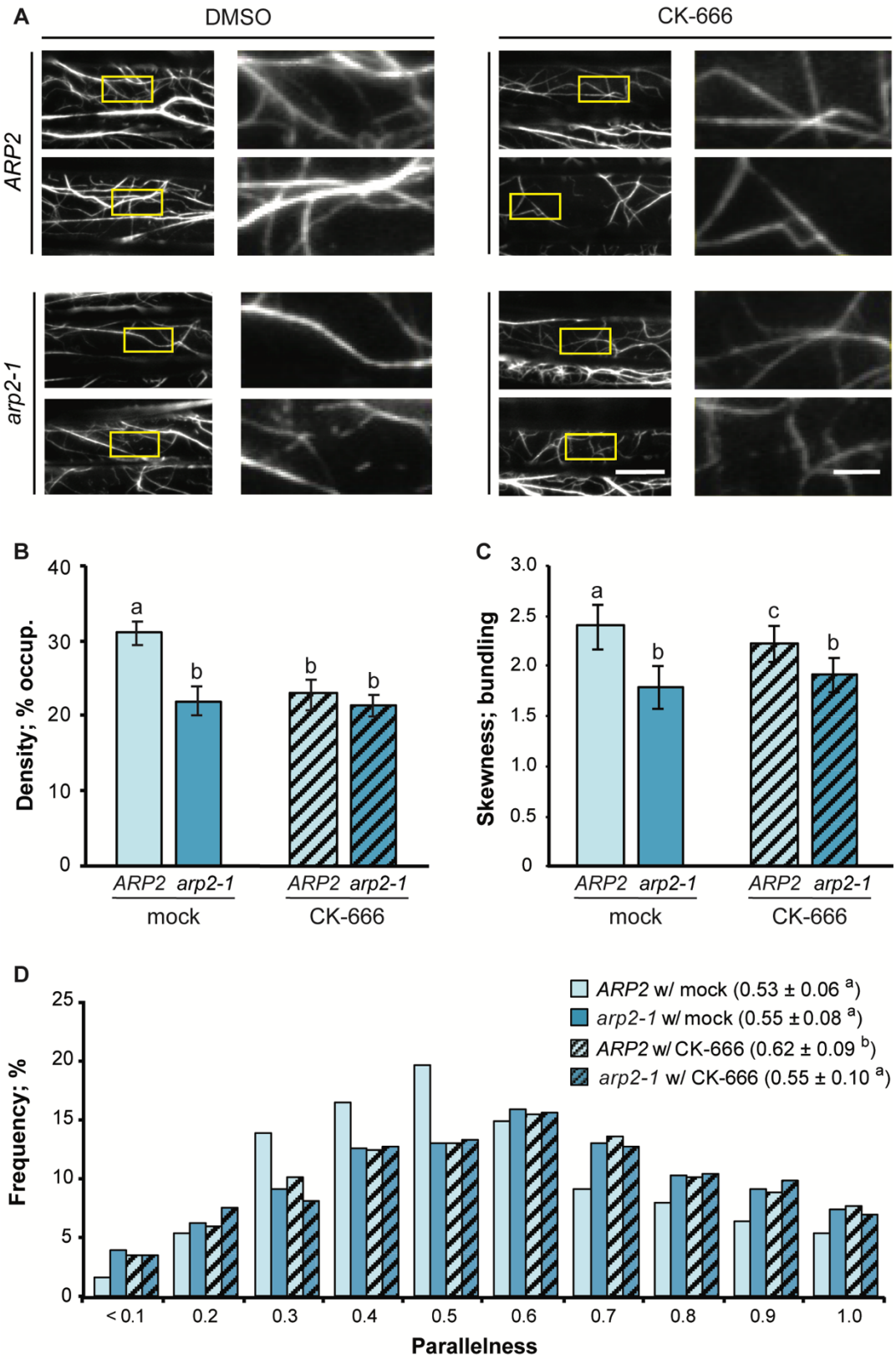
A
DMSO
CK-666
ARP2
arp2-1
B
Density; % occup.
40
30
20
10
0
a
b
b
b
ARP2 arp2-1
mock
ARP2 arp2-1
CK-666
C
Skewness; bundling
3.0
2.5
2.0
1.5
1.0
0.5
0
a
b
c
b
ARP2 arp2-1
mock
ARP2 arp2-1
CK-666
D
Frequency; %
25
20
15
10
5
0
ARP2 w/ mock (0.53 ± 0.06 a)
arp2-1 w/ mock (0.55 ± 0.08 a)
ARP2 w/ CK-666 (0.62 ± 0.09 b)
arp2-1 w/ CK-666 (0.55 ± 0.10 a)
< 0.1
0.2
0.3
0.4
0.5
0.6
0.7
0.8
0.9
1.0
Parallelness

Figure 5. A small molecule inhibitor of the Arp2/3 complex, CK-666, reduces filament density and bundling.

(A) Representative images of epidermal cells from the apical region of 5-day-old etiolated hypocotyls were shown in the left column. Bar = 20 µm. Regions of interest (yellow box) in left figures were magnified as shown in the right column. Bar = 5 um. Hypocotyls were treated with mock solution (0.05% DMSO) or 10 µM CK-666 for 5 min. prior to imaging with VAEM. Actin filament arrays in mock-treated *arp2-1*, CK-666-treated *ARP2*, and CK-666-treated *arp2-1* cells appeared to be less dense and less bundled compared to mock-treated wild-type cells. **(B)** and **(C)**, Quantitative analysis of the percentage of occupancy or density of actin filament arrays **(B)** and the extent of filament bundling or skewness **(C)**. Both the density and bundling of actin arrays in mock-treated *arp2-1*, CK-666-treated wild type, and CK-666-treated *arp2-1* cells were significantly decreased compared to mock-treated wild-type cells. **(D)** Quantitative analysis of the population distribution and average parallelness of actin filaments in hypocotyl epidermal cells. The average filament parallelness of CK-666-treated wild-type cells (*ARP2*) was significantly higher than others. In addition, the population distributions of mock-treated *arp2-1*, CK-666-treated wild type, and CK-666-treated *arp2-1* were all more left skewed compared to the mock-treated wild type. Values in **(B)** to **(D)** represent mean ± SE. n ≥ 300 cells from at least 15 hypocotyls per treatment or genotype (One-way ANOVA with Tukey's post-hoc test, letters [a-c] denote treatments or genotypes that show statistically significant differences with others, $P < 0.05$).

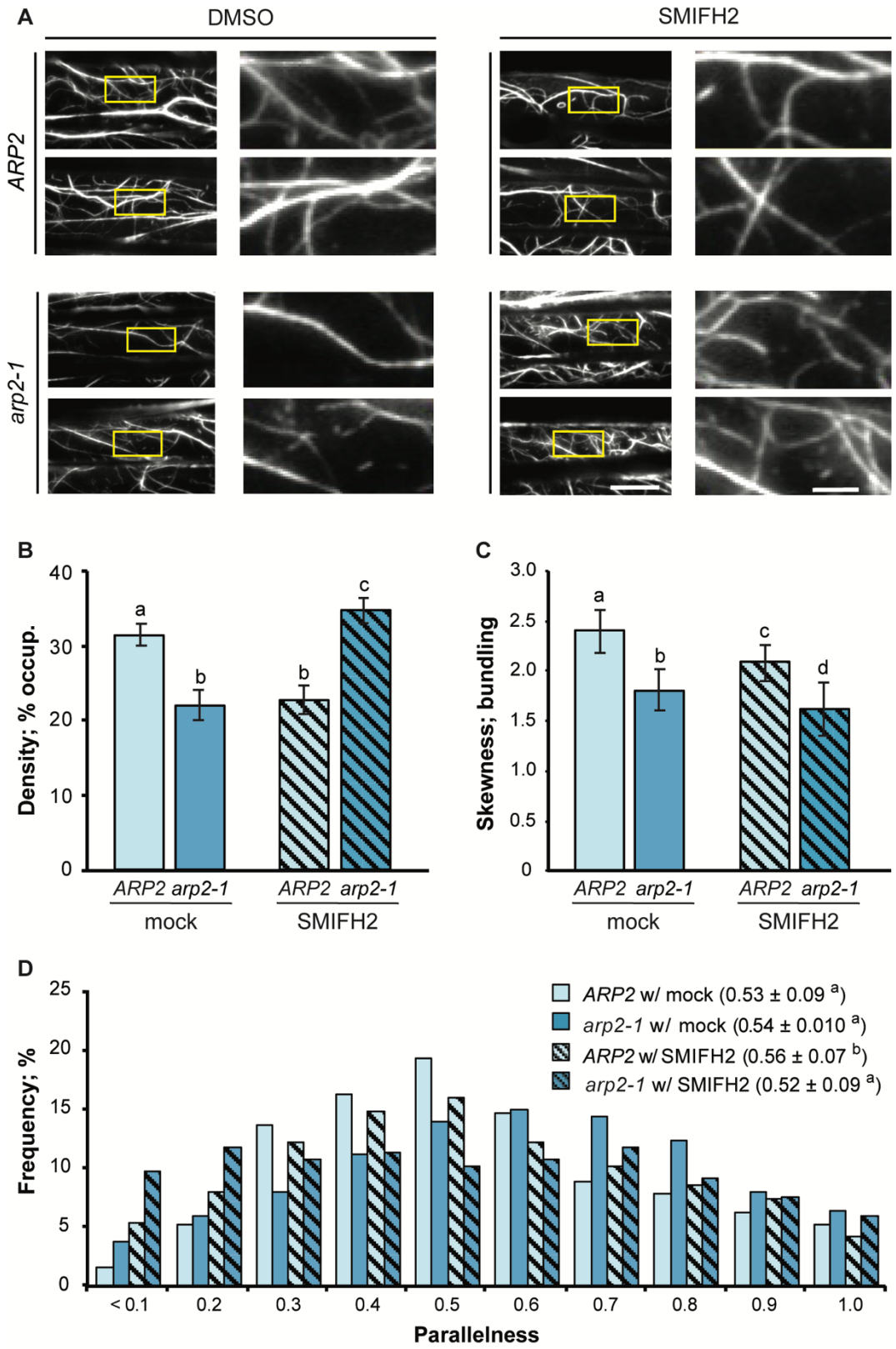
A
DMSO
SMIFH2
ARP2
arp2-1
B
Density; % occup.
40
30
20
10
0
a
b
b
c
ARP2 arp2-1
ARP2 arp2-1
mock
SMIFH2
C
Skewness; bundling
3.0
2.5
2.0
1.5
1.0
0.5
0
a
b
c
d
ARP2 arp2-1
ARP2 arp2-1
mock
SMIFH2
D
Frequency; %
25
20
15
10
5
0
ARP2 w/ mock (0.53 ± 0.09 a)
arp2-1 w/ mock (0.54 ± 0.010 a)
ARP2 w/ SMIFH2 (0.56 ± 0.07 b)
arp2-1 w/ SMIFH2 (0.52 ± 0.09 a)
< 0.1
0.2
0.3
0.4
0.5
0.6
0.7
0.8
0.9
1.0
Parallelness

Figure 6. Actin filament density significantly increases after treatment of *arp2-1* with the formin inhibitor SMIFH2.

(A) Representative images of epidermal cells from the apical region of 5-day-old etiolated hypocotyls were shown in the left column. Bar = 20 µm. Regions of interest (yellow box) in left figures were magnified as shown in the right column. Bar = 5 um. Hypocotyls were treated with mock solution (0.05% DMSO) or 25 µM SMIFH2 for 5 min. prior to imaging with VAEM. Actin filament arrays in mock-treated *arp2-1*, CK-666-treated *ARP2*, and CK-666-treated *arp2-1* cells appeared to be less dense and less bundled compared to mock-treated wild type cells. **(B)** to **(C)**, Quantitative analysis of density **(B)** and skewness **(C)**. **(B)** The density of actin arrays in mock-treated *arp2-1* and SMIFH2-treated wild type was significantly decreased compared to mock-treated wild type; however, SMIFH2-treated *arp2-1* cells had significantly increased actin density compared to other genotypes and treatments. **(C)** Actin arrays in *arp2-1* cells were significantly less bundled compared to wild-type cells (both mock- and SMIFH2-treated). **(D)** Quantitative analysis of the population distribution and average parallelness of actin filaments. The average parallelness of actin filaments in SMIFH2-treated wild-type cells is slightly higher than other genotypes and treatments; however, the distribution of SMIFH2-treated *arp2-1* was more right skewed compared to other genotypes and treatments. Values in **(B)** to **(D)** represent mean ± SE. $n \geq 300$ cells from at least 15 hypocotyls per treatment (One-way ANOVA with Tukey's post-hoc test, letters [a-d] denote treatments or genotypes that show statistically significant differences with others, $P < 0.05$).

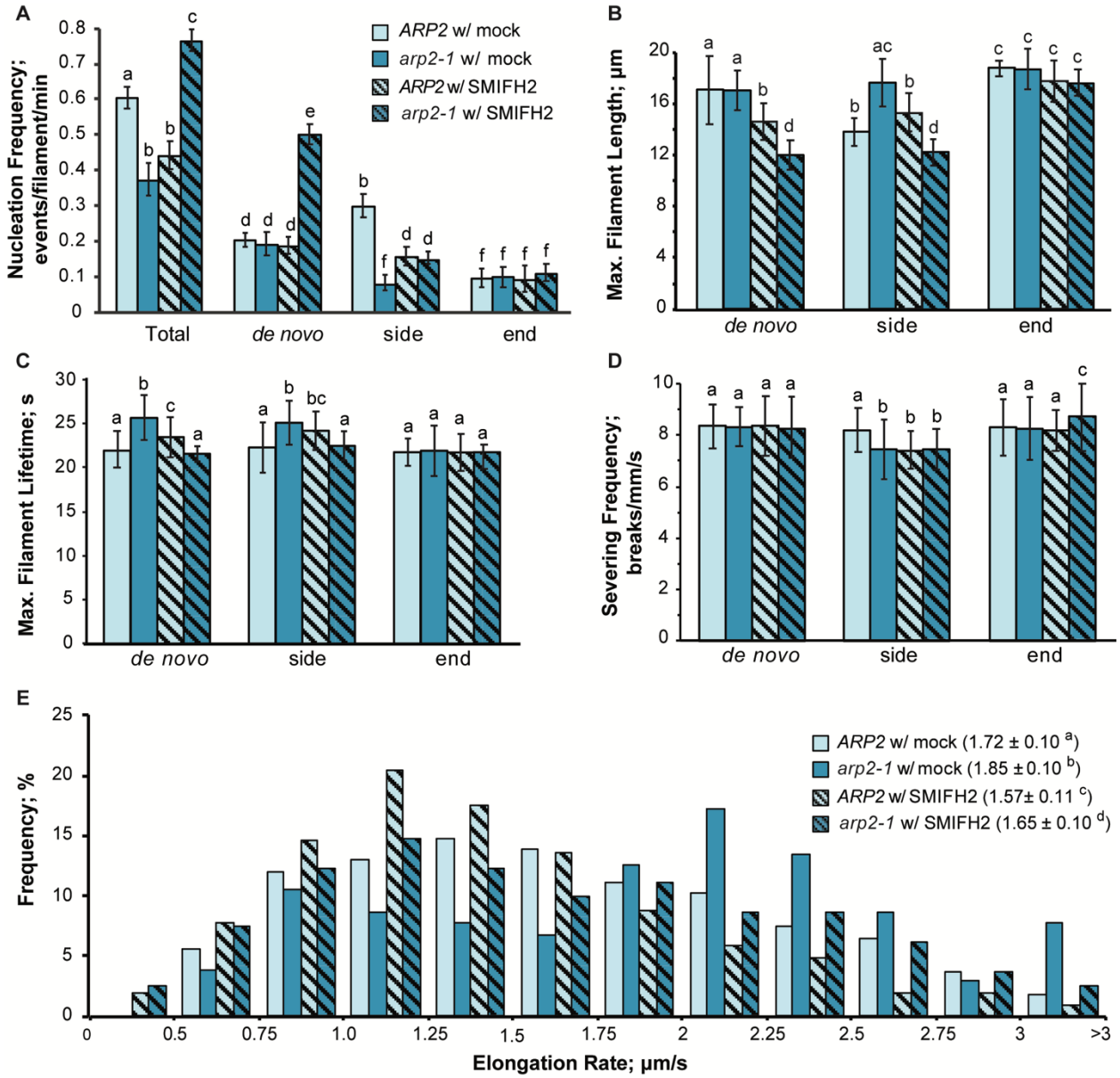

Figure 7. Overall and *de novo* filament formation increase when Arp2/3 and formin activity are simultaneously inhibited.

(A) Quantitative analysis of actin filament nucleation frequency, both overall and by subclass of origin. The total nucleation frequency in mock-treated *arp2-1* and SMIFH2-treated wild-type cells was significantly reduced compared to mock-treated wild-type (*ARP2*) cells. However, the total nucleation frequency of SMIFH2-treated *arp2-1* cells was significantly higher than all other genotypes and treatments and this correlated with increased *de novo* nucleation events. Values represent mean ± SE. n ≥ 350 total events from at least 15 hypocotyls per treatment or genotype (One-way ANOVA with Tukey's post-hoc test, letters [a-f] denote treatments or genotypes that show statistically significant differences with others, $P < 0.05$). **(B)** Average maximum length of filaments that originated *de novo* or from side-branching events in SMIFH2-treated *arp2-1* were significantly shorter than the ones from other cells, but filaments that originated from pre-existing ends did not show a difference between any genotype or treatment. **(C)** Average maximum lifetime of side-branching filaments in both mock-treated *arp2-1* and

SMIFH2-treated wild-type were significantly longer than the ones from mock-treated wild-type and SMIFH2-treated *arp2-1* cells. Filaments that were nucleated *de novo* in SMIFH2-treated *arp2-1* cells were significantly shorter than *de novo* filaments from other genotypes or treatments. **(D)** Side-branching filaments in mock-treated wild-type cells had a significantly higher severing frequency than the ones from other cells and end-growing filaments in both SMIFH2-treated wild-type and SMIFH2-treated *arp2-1* cells had significantly higher severing frequency than the ones from mock-treated cells. **(E)** Analysis of the population distribution of actin filament elongation rates. The average elongation rate for filaments from mock-treated *arp2-1*, SMIFH2-treated wild-type, and SMIFH2-treated *arp2-1* cells was significantly higher than mock-treated wild type. The elongation rate distribution of mock-treated wild type had a single peak at 1.25 – 1.5 µm/s, the mock-treated *arp2-1* had three peaks at 0.75 – 1.0 µm/s,2.0 – 2.25 µm/s and > 3 µm/s, the SMIFH2-treated wild-type had a peak at 1.0 – 1.25 µm/s, but SMIFH2-treated *arp2-1* had peaks at 1.0 – 1.25 µm/s and 1.75 – 2.0 µm/s. Values in **(B)** to **(E)** represent mean ± SE. n ≥ 50 single filaments from at least 10 hypocotyls per treatment (One-way ANOVA with Tukey's post-hoc test, letters [a-d] denote treatments that show statistically significant differences with other treatments, $P < 0.05$).

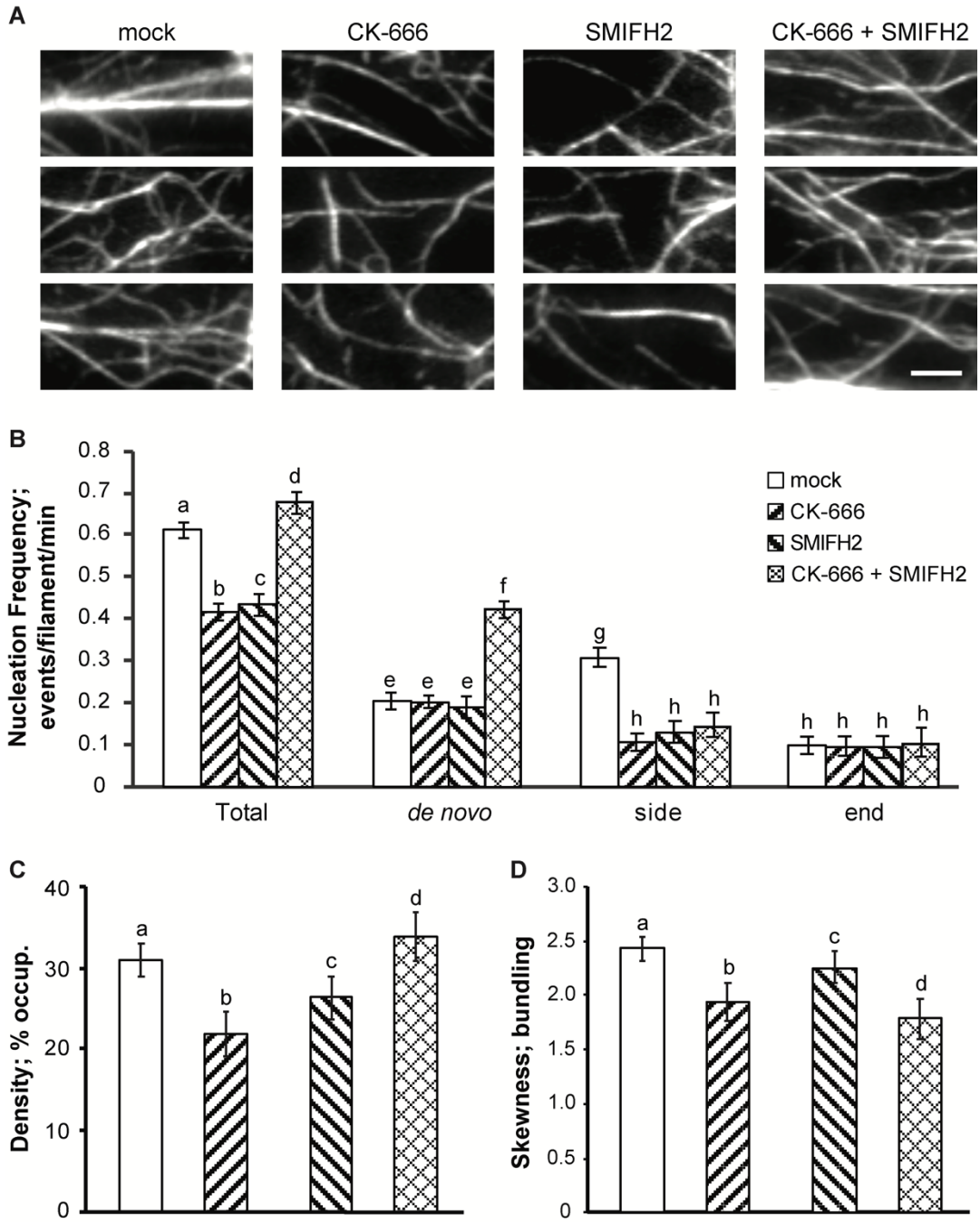

Figure 8. Filament abundance, total nucleation events and *de novo* filament formation increase when the Arp2/3 complex and formin activity are simultaneously reduced with inhibitors.

(A) Representative images of wild-type Col-0 hypocotyl epidermal cells expressing GFP-fABD2 after treatment with mock solution (0.1% DMSO), 10 µM CK-666, 25 µM SMIFH2, or both CK-666 and SMIFH2 for 5 min. prior to imaging with VAEM. Actin filament arrays in CK-666-treated cells and SMIFH2-treated cells appeared to be less dense and less bundled compared to mock-treated cells. However, dual treatment significantly increased actin filament abundance. Bar = 10 µm. **(B)** Quantitative analysis of actin filament nucleation frequency, both overall and by subclass of origin. The total

nucleation frequency in mock-treated cells was higher than CK-666-treated and SMIFH2-treated cells. However, the total nucleation frequency of dual-treated cells was significantly higher than other treatments and this correlated with increased *de novo* and side-branching nucleation events. Values in **(B)** represent mean ± SE. n ≥ 350 total events from at least 15 hypocotyls per treatment (One-way ANOVA with Tukey's post-hoc test, letters [a-h] denote treatments that show statistically significant differences with other treatments, $P < 0.05$). **(C)** and **(D)**, Quantitative analysis of density **(C)** and skewness **(D)** of actin filaments. **(C)** The density of actin arrays in CK-666-treated and SMIFH2-treated cells was decreased compared to mock-treated cells; however, dual-treated cells had significantly increased actin density compared to other treatments. **(D)** Actin arrays in CK-666- or dual-treated cells were significantly less bundled than in mock-treated cells. Values in **(C)** and **(D)** represent mean ± SE. n ≥ 300 cells from at least 15 hypocotyls per treatment (One-way ANOVA with Tukey's post-hoc test, letters [a-d] denote treatments that show statistically significant differences with other treatments, $P < 0.05$).